δ-Peptide Analogues of Pyranosyl-RNA

Part 2[1])

Nucleo-δ-peptides Derived from Conformationally Constrained Nucleo-δ-amino Acids: NMR Study of the Duplex Formed by Self-pairing of the (1′*S*,2′*S*,4′*S*)-(phba)-Nucleo-δ-peptide-(AATAT)[2])[3])

by **Harald Schwalbe**[a])[4])*, **Jochen Wermuth**[b]), **Christian Richter**[a]), **Sandor Szalma**[c]), **Albert Eschenmoser**[d]), and **Gerhard Quinkert**[a])

[a]) Institut für Organische Chemie der Universität, Marie-Curie-Strasse 11, D-60439 Frankfurt am Main
[b]) *Aventis Research & Technologies*, D-65926 Frankfurt am Main
[c]) *Molecular Simulations Inc.*, 9685 Scranton Rd., San Diego, CA-92121, USA
[d]) Laboratorium für Organische Chemie, Eidgenössische Technische Hochschule, ETH-Zentrum, Universitätstrasse 16, CH-8092 Zürich, and The *SKAGGS* Institute for Chemical Biology at The *SCRIPPS* Research Institute, 10550 North Torrey Pines Road, La Jolla, CA-92037

Dedicated to *Horst Kessler* on the occasion of his 60th birthday

δ-Peptides of the type described in this series are analogues of pyranosyl-RNAs with respect to their capability of base pairing in the *Watson-Crick* mode. An NMR-based conformational analysis of the title duplex at various levels of sophistication has been carried out: at the level of qualitative conformational analysis, at that of quantitative conformational analysis, and at that of structure calculation using MD search of torsion-angle space. The duplex formed has an antiparallel arrangement of two complementary strands and is stabilized by *Watson-Crick* base pairing, as well as by interstrand π-π base stacking, dangling-end nucleobase interaction included.

1. Introduction. – 1.1. *General Introduction to this Series of Publications.* See [1]: 1.1. 1.2. *Introduction to Part 2*. Nucleo-δ-peptides (NDPs) are non-natural oligomers. Compared structurally to oligonucleotides, they lack the sugar-phosphate backbone. The two oligomer types are expected to resemble each other in base-pairing capability. Evidence for pairing of complementary NDP single strands [2], as well as the syntheses [1] and oligomerizations [2] of their component nucleo-δ-amino-acid monomers (NDAas), were covered. The constitutions and configurations of these single strands are unproblematic, thanks to the straightforward way of their preparation. This is not the case for their conformations, however, nor for the conformations and constellations[5]) of the duplexes arising from spontaneous association of two single strands.

---

[1]) Part 1: [1]; Part 3: [2].

[2]) From the postdoctdoral report of *J. W.* [3] and the Ph.D. thesis of *C. R.* [4].

[3]) Abbreviations used and not explained in this paper: *ap: anti*-periplanar, *sc: syn*-clinal; phba defines the $[(HO)_2P(=O)-O-(CH_2)_3-C=O]$ radical fixed to the N-terminal radical of a NDP. For acronyms of NMR, techniques see [5].

[4]) Present address: *Francis Bitter Magnet. Lab.*, Department of Chemistry, Massachusetts Institute of Technology, Cambridge, MA 02139, USA.

[5]) The term 'constellation'refers to the relative positioning in space of non-covalently interacting molecules in supermolecules; see [6][7].

Here, we report on the results of NMR-spectroscopic studies on the structure of the title duplex **(1)$_2$** and of the related tetramer **2**. The structures properly interpreted may lead to an understanding of NDPs' base-pairing behavior.

1 (1'*S*,2'*S*,4'*S*)-(phba)-NDP (AATAT)

2 (1'*S*,2'*S*,4'*S*)-NDP (ATAT)

1.3. *Qualitative Conformational Analysis.* Predicting the conformation of an NDP single strand may take as its starting point the known conformations of α-peptides. A qualitative conformational analysis[6]), based essentially on minimizing *Pitzer* and *Newman* strain[7]), locates the α-peptide global minimum in the idealized-linear conformation of *Fig. 1,a*.

This backbone conformation proves not only free of *Pitzer* and *Newman* strain, but also experiences no 1,3-allylic strain[8]), and is optimally preorganized for supramolecular self-organization into pleated sheets.

The four centers C^{α}_{i-1}, C_{i-1}, N_i, and C^{α}_{i} of the α-peptide backbone, together with their bonds to H^{α}_{i-1}, O_{i-1}, H_i and H^{α}_{i}, lie in a plane. This has the result that any two such bonds at adjacent centers are *ap*-oriented, while those at centers next but one to each other are of parallel orientation.

The $C^{\alpha}_{i}-H^{\alpha}_{i}$ bond is part of two neighboring planes. It is flanked on one side by the $C_{i-1}-O_{i-1}$ bond, and on the other by the $N_{i+1}-H_{i+1}$ bond. If three-dimensional space is assumed to be divided into two *half-spaces* by the plane including the C=O groups, then the side chains on the C^{α}-atoms of the α-peptides backbone change half-space in alternating fashion.

Application of this type of conformational analysis to δ-peptides gives the same backbone conformation as for α-peptides, with the exception that every second amide residue is replaced by an ethane-1,2-diyl element (*Fig. 1,b*). Instead of the α-peptide's linear four-center $C^{\alpha}_{i-1}-C_{i-1}-N_i-C^{\alpha}_{i}$ pattern (*Fig. 1,a*), in the δ-peptide we find the four centers $C^{\delta}-C^{\gamma}-C^{\beta}-C^{\alpha}$ in a zigzag arrangement (*Fig. 1,b*). While conformational flexibility in the resulting single strand is increased by this substitution, the propane-1,3-diyl bridge connecting the β- and δ-positions – and hence forming a conformationally rigid cyclohexane ring – then restricts it once again (*Fig. 1,c*). The cyclohexane rings not only consolidate the statics of the δ-peptide backbone, but in the favored backbone conformation they also align nucleobases in position 1′ of each NDP (*vide infra*) parallel to each other (see *Fig. 1,d*). The nucleobases adopt an equatorial orientation in the 1′-position on each cyclohexane ring, while carbamoylmethyl bridges connect the 2′- and 4′-positions of adjacent cyclohexane rings, again in equatorial orientation (*Fig. 2*).

Of the six torsion angles that determine the idealized backbone of the conformationally restricted NDP (*Fig. 3*, *c* and *d*), three (γ, δ, and ζ) are predetermined from the outset. Torsion angles γ and δ or ζ specify the spatial arrangement of two outer atoms

---

6) For qualitative conformational analysis of α-peptides, see [8]: Chapt. 7.3.3.2.

7) The term '*Newman* strain' refers to excess enthalpy of a molecule, caused by the ($\pm sc, \mp$ sc)-conformational type with two successive torsion angles of the same magnitude (60°), but inverted signs. For coinage and extensive use of the term, see [8].

8) The term '1,3-allylic strain' was coined by *F. Johnson* [9] and widely used by *R. W. Hoffmann* [10]; see also Chapt. 7.3.3.2.2 in [8].

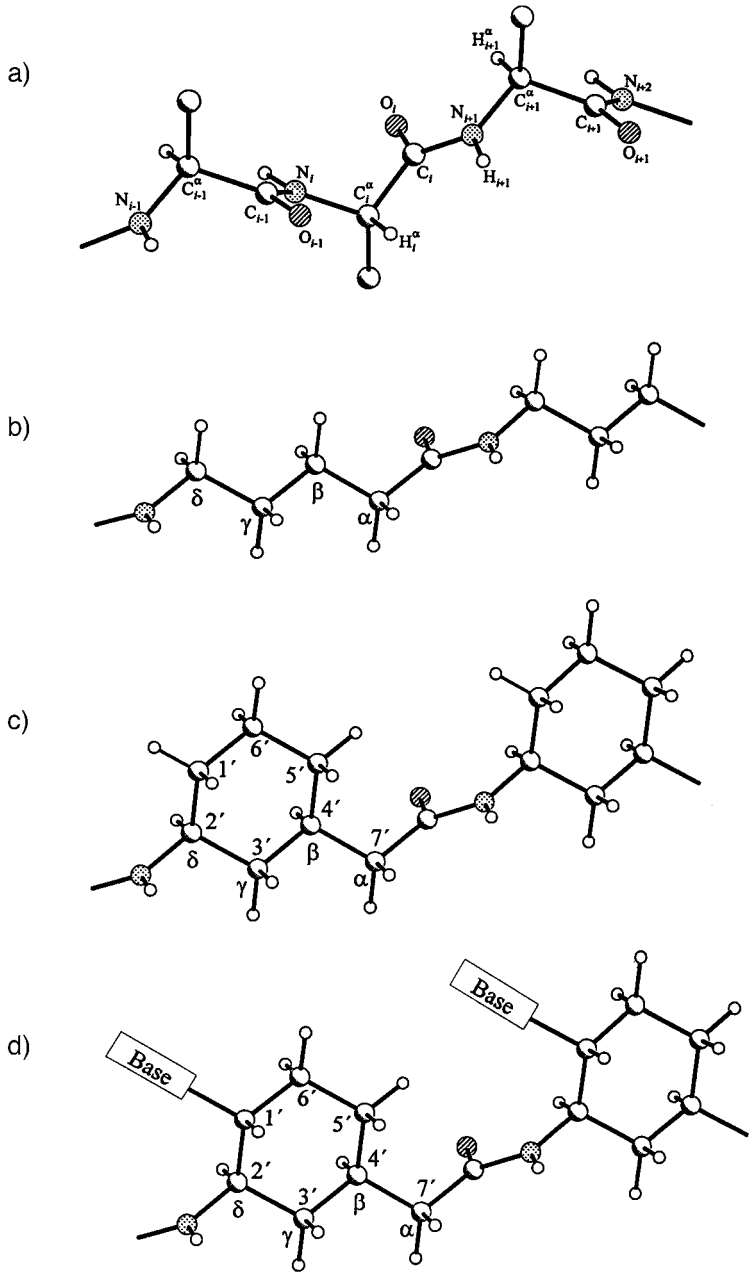

Fig. 1. *Segments of idealized backbones of* a) *α-peptide* (with torsion angles $\varphi = -120°$, $\psi = 120°$, $\omega = 180°$); b) *δ-peptide, unconstrained*, c) *δ-peptide, constrained by a propan-1,3-diyl group bridging β- and δ-positions*; d) *constrained δ-peptide with a nucleobase in 1′-position*

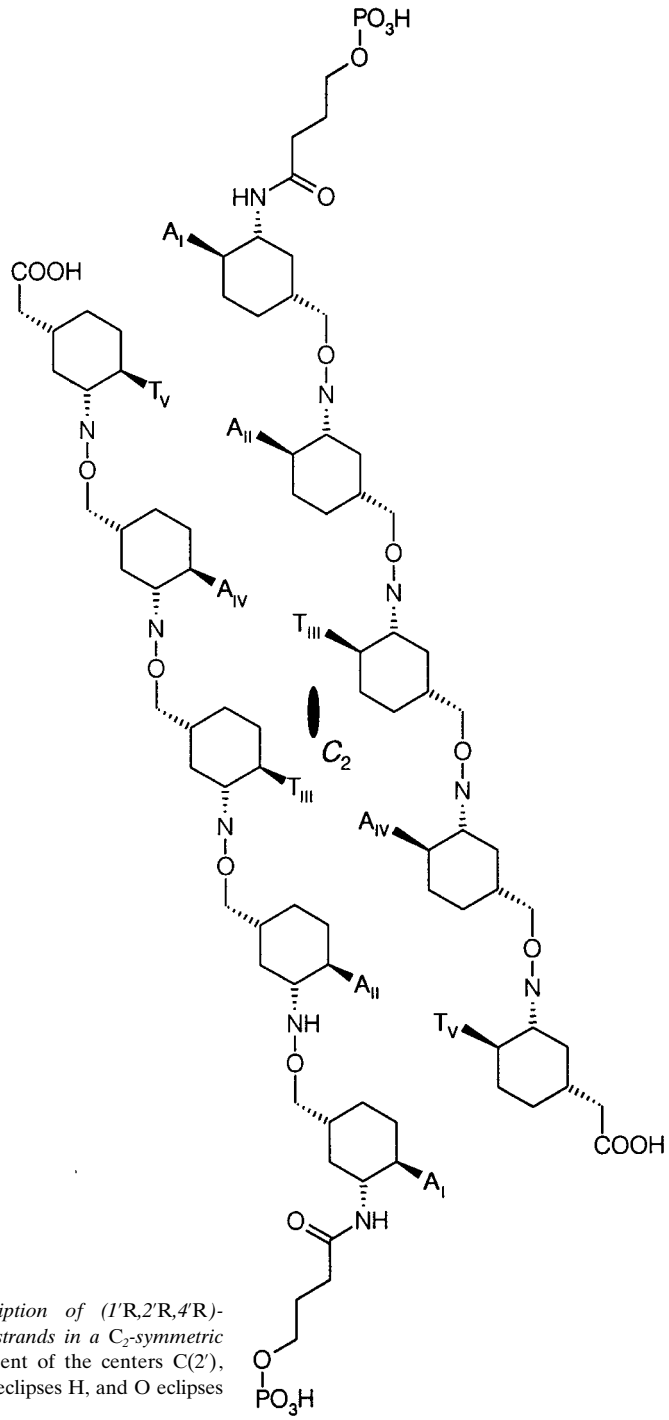

Fig. 2. *Bird's eye view description of (1′*R,*2′*R,*4′*R*)-(phba)-NDP (AATAT) single strands in a* C_2*-symmetric duplex.* In the linear arrangement of the centers C(2′), N(−H), C(=O), and C(4′), N eclipses H, and O eclipses C.

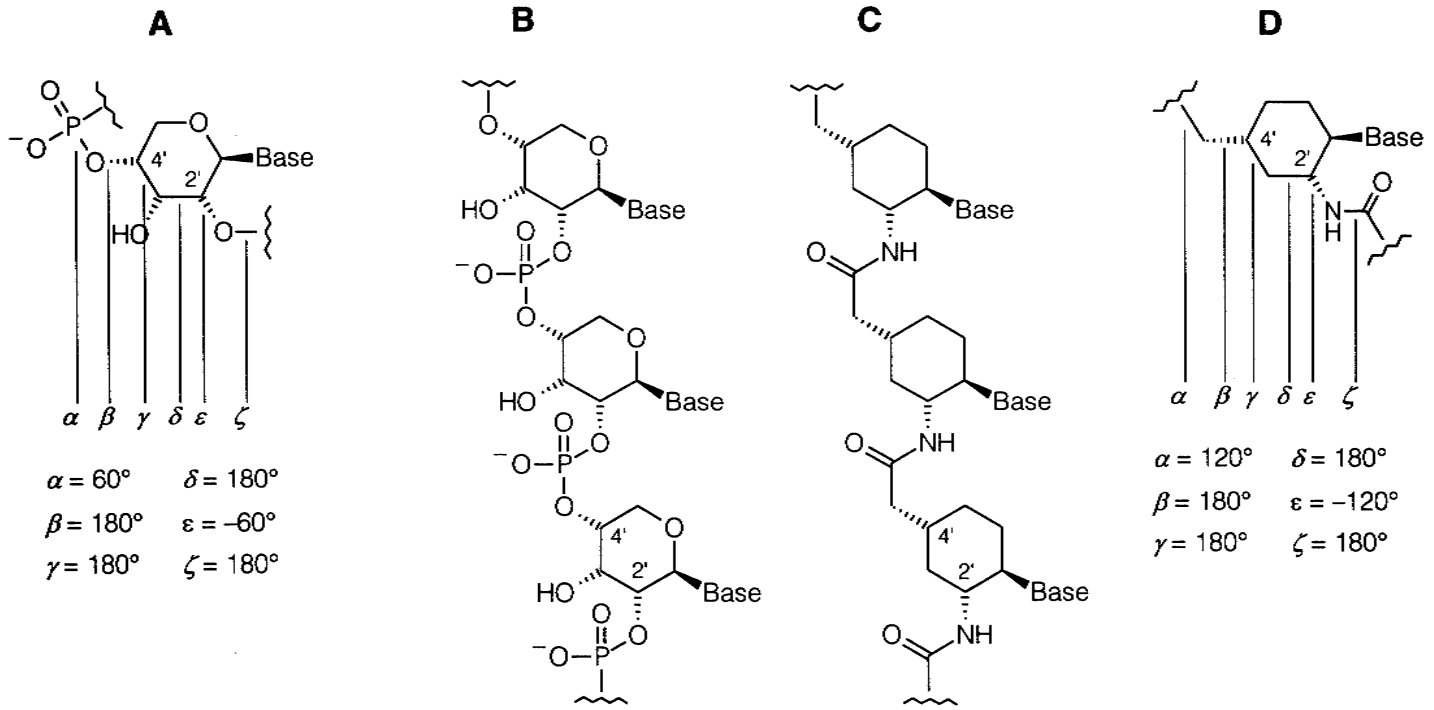

Fig. 3. *Sections of p-RNA* (b) *and (1'*R,*2'*R,*4'*R*)-NDP* (c) *with specification and numerical data for the torsion angles in the repeating units* a *and* d *of the two oligomers*

along a bond of the rigid ring between two inner atoms or along the peptide bond, respectively. Each amounts to 180°. In the thermodynamically favored conformation, angle β also adopts the value of 180°. Torsion angles α and ε, on the other hand, are both 120°.

In pyranosyl-RNA (p-RNA) [11] (*Fig. 3*, *a* and *b*), the model for NDP[9]), the corresponding torsion angles are: $\alpha = 60°$, $\beta = \gamma = \delta = 180°$, $\varepsilon = -60°$, and $\zeta = 180°$ (*Fig. 3*). Comparing these two oligomer types, torsion angles α and ε can be seen to differ in numerical value (120° in NDP, 60° in p-RNA). Within either one oligomer type, though, they differ only in sign. In the latter case, individual influences of torsion angles deviating from 180° offset each other in the overall conformation of the relevant backbone. Although the bridge elements between two adjacent six-membered rings in p-RNA (sugar-phosphate residue) and in NDP (carbamoylmethyl residue) differ from one another constitutionally and conformationally, superimposed projections of the six-membered rings and their nucleobases show them adopting the same positions in space, assuming the inclinations between the average base-pair axis and the idealized-linear strand axis have the same direction[10]). As this inclination is very pronounced in NDP (as in p-RNA) in comparison with the naturally occurring nucleic acids in the quasi-linear duplex, it is possible to accommodate only those constellations, in which the single strands are oriented in antiparallel fashion (see *Fig. 2*) and interstrand base stacking contributes more to stabilization than intrastrand base stacking[11]).

In the light of this comparative conformational analysis of p-RNA and NDP, hybridisation of the (1′*S*,2′*S*,4′*S*)-nucleo-δ-peptide single strand of sequence $(T)_4$ and the [β-L-ribopyranosyl-(2′→4′)-oligonucleotide] single strand of sequence $(D)_6$ (D = 2,6-diaminopurine = purine-1,2-diamine) described in *Part 3* of this series [2] is not surprising. Qualitative conformational analysis-based predictions relating to conformations of duplexes of p-RNA strands are in good agreement with the findings of *Jaun* and *Schlönvogt*'s NMR-spectroscopic studies of the duplex formed from β-D-ribopyranosyl-(2′→4′) single strands of sequence (CGAATTCG) [11c].

Accordingly, we studied the NDP duplex **(1)$_2$** with the aid of 1D- and 2D-NMR techniques, assigning the numerous resonance signals recorded to the protons causing them. On the basis of NOE data and homonuclear vicinal coupling constants, a quantitative conformational analysis study was carried out (see *Chapt. 2*). Furthermore, to make optimal use of the full wealth of obtained NMR data, the structure of **(1)$_2$** was calculated using a molecular dynamics simulation (see *Chapt. 3*). For this, we applied a modification of a routinely used algorithm [13] to process the simulated molecular dynamics (MD) in the torsion angle space (see *Sect. 3.1*).

2. NMR Spectroscopy of (1)$_2$ and 2. – While tetramer **2** is suitably soluble in a H_2O/MeCN 4:1 mixture, it was found convenient to phosphorylate pentamer **1** for temper-

---

[9]) An extensive investigation of p-RNA's structural and chemical properties has been extended to the whole family of diastereoisomeric pentopyranosyl-(2′→4′)-oligonucleotide systems [11d].

[10]) The inclination between (standardized) backbone and base-pair axes is negative in the case of β-ribopyranosyl-(2′→4′)-oligonucleotides. This also holds true for the nucleo-δ-peptides currently of interest; for further details, see [2][12].

[11]) Interstrand π-π base stacking correlates conformationally with a pronounced inclination of an oligomer backbone toward the base-pairing axes [11d][12].

ature-dependent NMR examination. Phosphorylation was performed at the N-terminus after introduction of a 4-hydroxybutanoic acid linker, designated below as hba.

2.1. *Nomenclature and Symbols.* For convenience, A and T specify the residues of nucleobases adenine and thymine[12]), respectively. Their position in a sequence, for assignment of relevant protons and their through-space interactions with other protons in the vicinity, is indicated by a Roman numeral in a clearly marked case or by a sequential term in a general case (*Fig. 4*). Numbering of nucleobases starts at the N-terminus, written to the left. The absolute configuration at each stereogenic center is given by the (*R*,*S*)-convention of the *CIP* system. The name for single strand **2**, for example, is (1′*S*,2′*S*,4′*S*)-NDP-($A_I T_{II} A_{III} T_{IV}$). A shortened notation is used here to specify the H atoms (*e.g.*, H1′ = H−C(1′)).

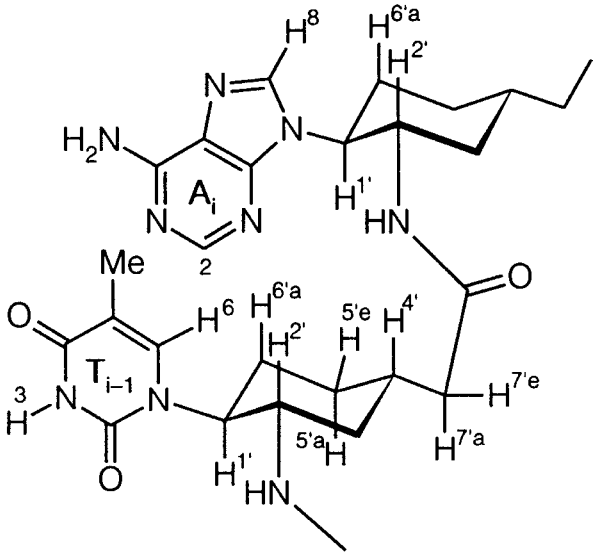

Fig. 4. *Sections of a (1′*S*,2′*S*,4′*S*)-NDP single strand with specification of protons relevant for NMR-based conformational analysis*

In *Sect. 1.2*, because of close relationship of β-D-ribopyranosyl-(2′ – 4′)-oligonucleotides to (1′*R*,2′*R*,4′*R*)-nucleo-δ-peptides, we have actually been talking of the (all-*R*)-enantiomer of the latter (see *Fig. 1*,*d*, *Fig. 2*, and *Fig. 3*). Because of practical reasons, however, the (all-*S*)-enantiomers $\mathbf{(1)_2}$ and **2** have been studied NMR-spectroscopically.

2.2. *Resonance Assignments and Evidence for Base Pairing.* Considering the conformational problems requiring later resolution (see *Sect. 2.3*), structural determination of $\mathbf{(1)_2}$ poses the following three questions for NMR analysis: *1*) Which resonance signals should be assigned to which individual protons in the spin systems of the cyclohexyl residues present? *2*) Which of the five cyclohexyl residues is bound to which of the five nucleobase residues, and what position does the resulting NDAa residue occupy in the sequence of the single strand? *3*) What base pairings exist in a duplex formed from complementary NDP single strands?

---

[12]) In Part 3 [2], A and T refer to NDAa residues. In Part 1 [1], adenine and thymine are abbreviated conventionally as Ade and Thy.

The protons in the cyclohexyl system can be assigned, H7′ protons included, with no great difficulty. Since all three substituents are positioned equatorially (or put another way, H1′, H2′, and H4′ occupy axial positions), the choice of the starting point is relatively simple. Analysis hinges on the relevant amide proton and its interactions with several protons in its vicinity, either through space or over three bonds with H2′.

The order of the A and T nucleobases may be determined from the fact that: *1*) the H6 protons in T and the H8 protons in A, whose resonance signals are significantly far removed from one another, interact through space with H6′ and H2′ protons, thus enabling a given nucleobase and associated cyclohexyl residue to be joint together into one and the same NDAa residue; *2*) the H5′ protons of NDAa residues adjoining an A-base in the direction of the C-terminus are exposed to the ring current effect, and *3*) the terminal NDAas can be recognized by their functional groups.

Finally, the base pair characterizing the duplex can be ascertained experimentally through comprehensive measurement of through-space proton-proton interactions.

It is expected that these broadly indicative remarks will serve to enable interpretation of the findings obtained through various different NMR techniques to be followed more comfortably.

According to 2D-^{1}H-jump-return experiments, self-complementary single strands **1** form the C_2-symmetric duplex **(1)$_2$** (see *Fig. 2*) in solution (H_2O/^2H_2O 9:1, 10 mM K_2HPO_3, pH 5.5) at a temperature of 286 K: *Fig. 5* shows only two imino resonances. The sharper of the two imino resonance signals for T – at 12.1 ppm – may, from analysis of the 2D-^{1}H-jump-return NOESY spectrum (*T* 275 K), be assigned to the imino proton of T_{III} of the inner base pair, the broader – at 11.4 ppm – to that of T_V of the outer base-pair. The outer base pair (T_V,A_{II}) is weaker than the inner base pair (T_{III},A_{IV}), and exchange with water takes place more easily in the former case than in the latter.

NMR Spectra of **2** were measured in a mixture of H_2O/C^2H_3CN 4:1. A section of the 1D-^{1}H-NMR spectrum of **2**, showing the resonances of NH and of the ring protons of the nucleobases can be seen in *Fig. 6*,*a*. The resonances of base protons T-H6, and A-H8 are clearly resolved. The doublet splitting of the resonances of the three amide protons of T_{II}, A_{III}, and T_{IV} are plainly discernible, and represent a ^3J(NH,H2′) value of *ca*. 10 Hz. In place of the amide protons in the N-terminal A_I of **(1)$_2$**, A_I of **2** under the given conditions shows non-resolvable ammonium protons. The resonance signals of the amide and amino protons are no longer evident after exchange of H_2O with ^2H_2O, and only observable in weakened state on saturation of the H_2O resonance. Imino resonances, indications of base pairing [14], are not observed. At temperatures below 273 K, pronounced line broadenings are observed for **2**. *A priori*, a self-paired duplex with a C_2 axis would be expected. This, however, is not in accord with the three imino protons observable at this temperature. An extended *Watson-Crick* pairing with one or more displaced strands would be compatible not only with the NMR-spectroscopic line-broadening data and symmetry properties the same as in the monomer, but also with the S_2-symmetric arrangement observed in the crystal structure of the DNA tetramer dpApTpApT [15], in which each tetramer enters into base pairing with two of the self-pairing molecules.

In the 1D-^{1}H-NMR spectrum of **(1)$_2$** (*Fig. 6*,*b*), the following features, relative to **2** (*Fig. 6*,*a*), are noteworthy: *1*) the greater line width; *2*) the high-field shift of the aromatic signals, especially the A-H2-protons, attributable to ring current effects of

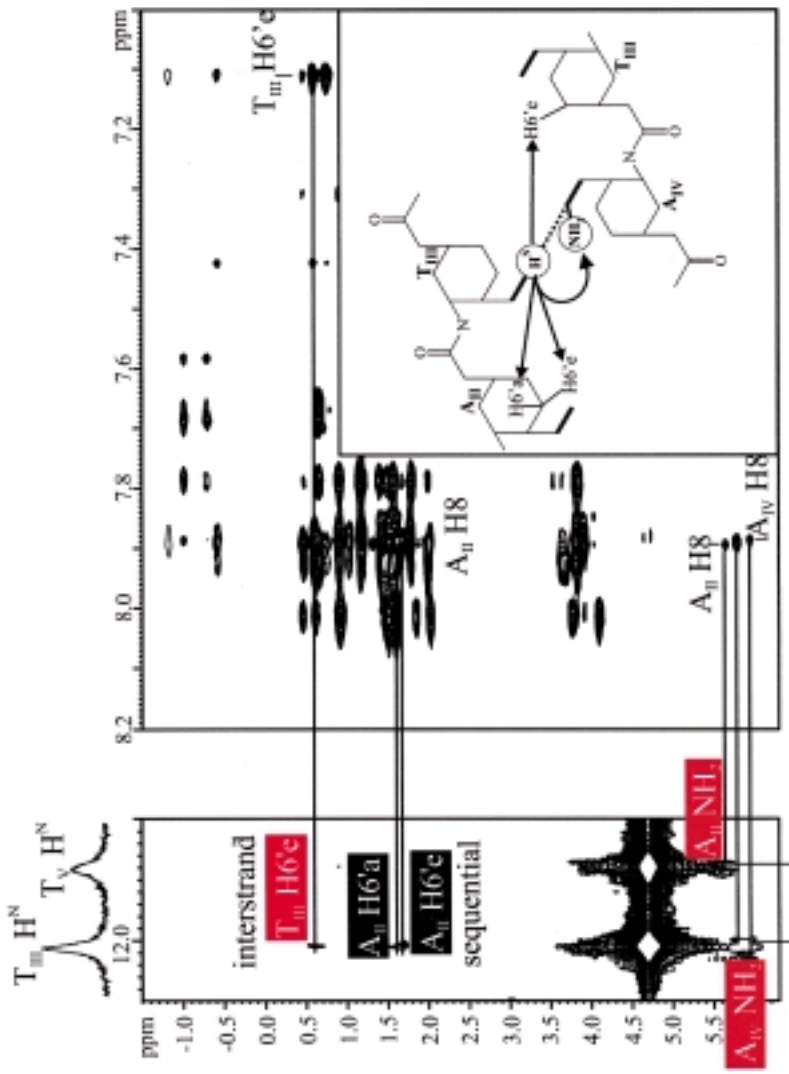

Fig. 5. *Selected region of the 2D-^{1}H-jump-return NOESY spectrum* (600 MHz) *of* **(1)$_2$** *in H_2O/H_2O 9 :1 at 277 K with the imino resonances of T_{III} and T_V at 12.1 and 11.4 ppm on top, taken from the 1D-^{1}H jump-return spectrum.* For better understanding, interstrand cross-peaks are indicated by red fields, intrastrand cross peaks by black fields. Intraresidual cross-peaks are shown without special marking. Intrastrand cross-peaks between the T_{III}-imino proton and A_{II}-H6′$_a$ or A_{II}-H6′$_e$, as well as interstrand cross-peaks between the T_{III}-imino proton and T_{III}-H6′$_e$, A_{II}- and A_{IV}-amino protons are visible (see formula in the box)

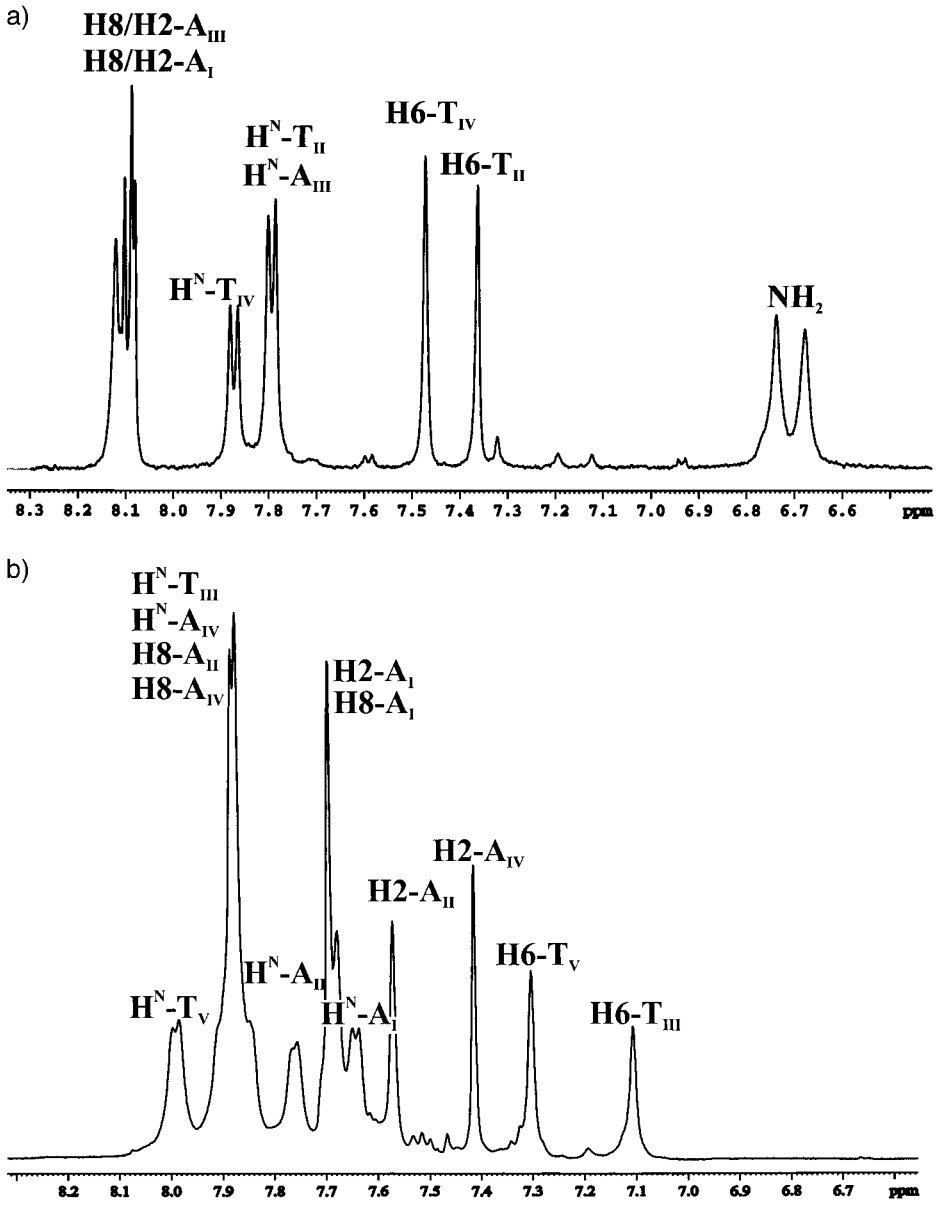

Fig. 6. *1D-^{1}H-NMR Spectra* (600 MHz) *showing the aromatic and amidic protons of* a) **2** *in* $H_2O/^2H_2O$ 4:1 *with traces of MeCN* (weak peaks due to a second conformation not further considered); b) $\mathbf{(1)_2}$ *in* $H_2O/^2H_2O$ *at 286 K*

nucleobases in the complementary single strand; *3*) the low-field shift of the amide protons.

Further assignment of the proton resonances of $\mathbf{(1)_2}$ and **2** was accomplished through analysis of 2D COSY [16], TOCSY [17], ROESY [18], and NOESY

experiments [19], while ^{13}C resonances were assigned using $^{1}H,^{13}C$-HSQC techniques [20].

Analysis of the NOESY spectrum of **(1)$_2$** (*Fig. 5*) suggests a C_2-symmetric duplex with *Watson-Crick* mode base pairing between complementary strands: for residues A_{II} and T_V, and also T_{III} and A_{IV} (see *Fig. 2*). The imino proton of T_{III} shows an intrastrand cross-peak to $H6'_e$ of the adjacent A_{II} and an interstrand cross-peak to $H6'_e$ from T_{III}. For this last cross-peak, it is not possible to decide on the basis of thespectrum whether an interstrand or an intraresidual correlation is responsible. Assignment can be made, however, on the basis of their different distances in the calculated duplex structure (*vide infra*). The distance from the imino proton to the intraresidual $H6'_e$-proton is 5.1 Å, while to the interstrand $H6'_e$ proton it is only 3.8 Å.

Finally, intrastrand cross-peaks (A_{IV}-NH_2/T_{III}-H6, and A_{II}-NH_2/A_I-H8) and also interstrand cross-peaks (A_{IV}-NH_2/A_{II}-H8 and A_{II}-NH_2/A_{IV}-H8) from the amino protons were observed.

Fig. 7 gives all the observed intrastrand (black correlation lines) and interstrand (red correlation lines) NOE interactions for **(1)$_2$**. NMR Analysis reveals the antiparallel orientation of the two strands, four A-T base pairings of *Watson-Crick* type and interstrand A_{II},A_{IV}, or A_{IV},A_{II} stacking interactions.

From the perspective of non-terminal adenyl residue H2 protons, three well-separated cross-peaks can be seen. ForA_{II}, these are an intraresidual cross-peak to A_{II}-H1′, an intrastrand to A_I-H1′, and an interstrand one to A_{IV}-H1′. Cross-peaks arising from A_{IV} participation are: A_{IV}-H2/A_{IV}-H1′ (intraresidual), A_{IV}-H2/T_{III}-H1′ (intrastrand), and A_{IV}-H2/A_{II}-H1′ (interstrand).

The COSY spectrum of **(1)$_2$** (*Fig. 8,b*) shows five well-resolved HN-H2′ cross-peaks at chemical shifts $\omega_1 \approx 3.7$ ppm and $\omega_2 \approx 7.8$ ppm. The HN resonances of T_{III} and T_V are found at lower field relative to those of A_I, A_{II}, and A_{IV}. The same trend can be observed in the COSY spectrum of the single strand **2** (*Fig. 8,a*).

While protons H1′ and H2′ in **(1)$_2$** and **2** resonate between 3.3 and 4.2 ppm (see *Tables 1* and *2*), and protons $H3'_a$/$H3'_e$, H4′ and $H6'_a$/$H6'_e$ for all NDAa residues resonate between 0.3 and 2.0 ppm, an appreciable high-field shift of the H5′-resonance signal is observed for those residues followed (in the direction of the C-terminus) by an A (A_I and T_{III} in **(1)$_2$**, and T_{II} in **2**). This amounts to *ca.* 2.7($H5'_e$)/1.4($H5'_a$) ppm relative to the H5′ resonances of the C-terminal T_V in **(1)$_2$** and 1.6($H5'_e$)/0.9($H5'_a$) ppm relative to the H5′ resonances of the C-terminal T_{IV} in **2**. In addition to this, the relative positions of the two diastereotopic protons $H5'_a$ and $H5'_e$ invert for these residues. The accepted rule for cyclohexane, that axial protons resonate at higher field than equatorial ones [21], is not followed in this instance. A shift to higher field, albeit less pronounced as for NDPs, is also observed for some $H5'_e$ protons (but not $H5'_a$ protons) in the case of pRNA, when they follow (in the p-RNA numbering scheme[13])) an adenine-pRNA repeating unit [11c].

Identification of *cyclohexyl ring* and *nucleobase* spin systems belonging to the same NDAa residue in **2** can be successfully performed by exploiting the following observations: The H6 protons in T_{II} and T_{IV} in **2**, which can be unambiguously

---

[13]) The differing repeating-unit numbering schemes for NDPs (N-terminus to C-terminus) and pRNAs (4′- to 2′-end) mean that formal strand directions are opposite in NDP and in pRNA.

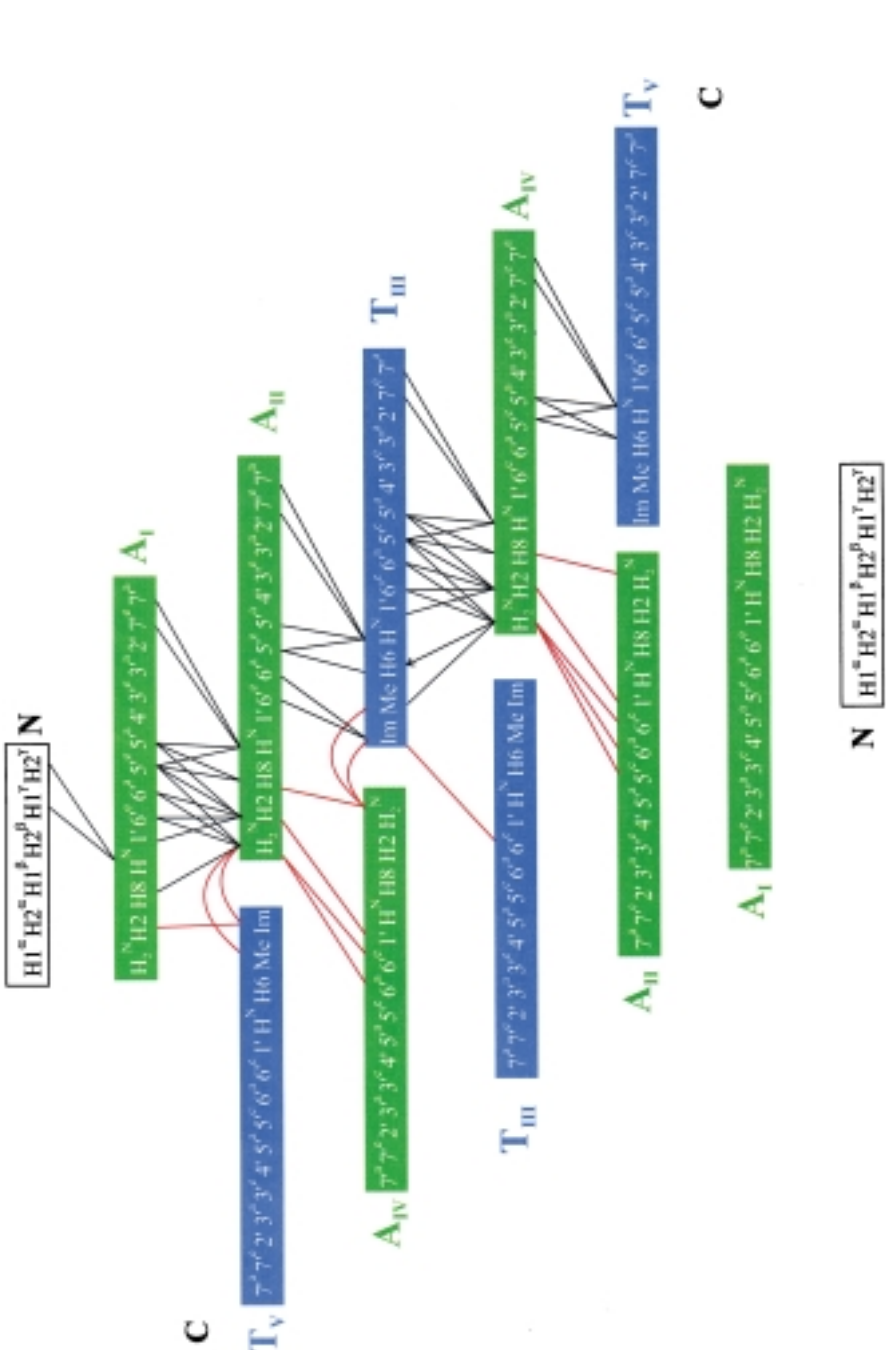

Fig. 7. *Outline of all observed intrastrand* (black lines) *and interstrand* (red lines) *NOE correlations extracted from cross-peaks in NOESY spectra of* **(1)**$_2$ *in* $H_2O/^2H_2O$ *9 : 1 and* ^2H_2O

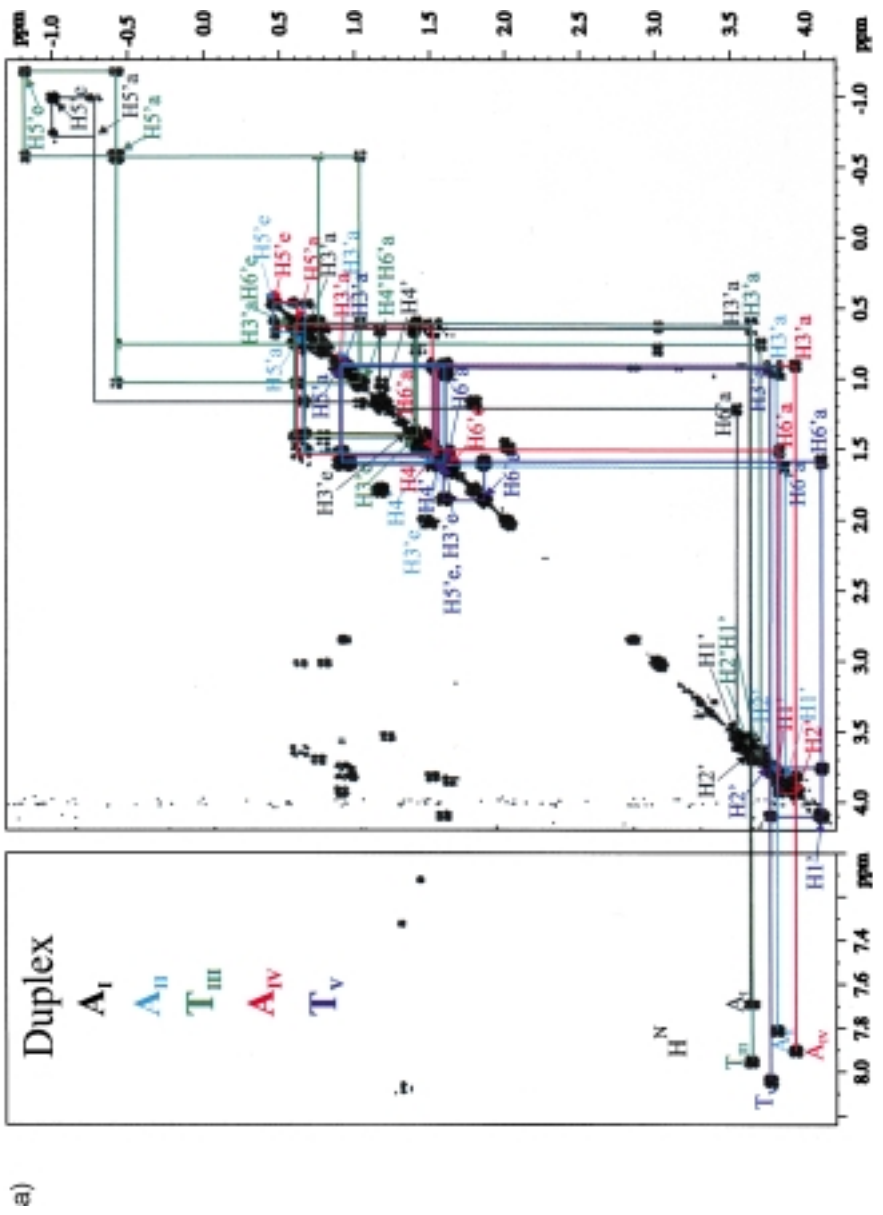

Fig. 8. *DQF-COSY Spectra* a) *of* $(\mathbf{1})_2$ *or* b) *of* **2**, *with indicated assignments of proton resonances*

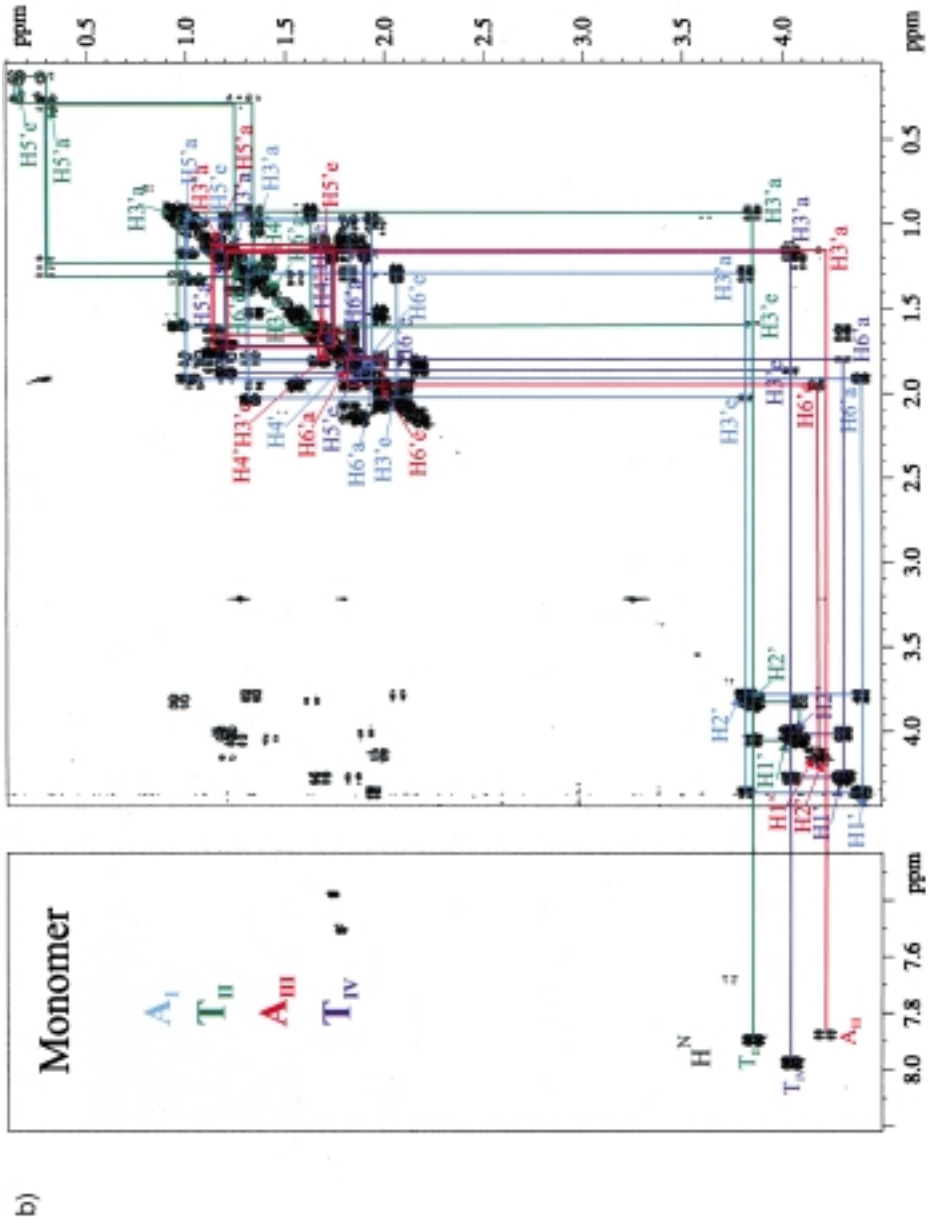

Fig. 8. (cont.)

Table 1. *^{1}H- and ^{13}C-NMR Chemical-Shift Values of* **(1)$_2$** (relative to TMS at 0 ppm) *in H_2O at 277 K*

	A_I	A_{II}	T_{III}	A_{IV}	T_V
NH	7.684	7.805	7.947	7.898	8.034
A-NH_2/T-N^3H		5.78/5.635	12.07	5.94/5.78	11.41
H2′	7.72	7.60		7.43	
H8,H6	7.72	7.898	7.126	7.908	7.328
H of Me			1.428		1.305
C of Me			22.86		22.63
H1′	3.531	3.839	3.690	3.812	4.092
C(1′)	68.35	67.72	67.87	67.69	67.69
H2′	3.629	3.799	3.629	3.924	3.756
C(2′)	59.50	63.09	59.50	62.36	60.88
$H3'_a$	0.648	0.903	0.605	0.903	0.913
C(3′)	47.90	48.18	48.39	48.43	49.11
$H3'_e$	1.391	1.580	1.413	1.571	1.613
H4′	1.162	1.520	1.028	1.530	1.59
C(4′)	43.08	44.02	43.45	44.02	44.94
$H5'_a$	– 0.717	0.671	– 0.578	0.614	0.948
C(5′)	38.07	39.73	38.34	39.73	41.56
$H5'_e$	– 0.996	0.461	– 1.180	0.451	1.61
$H6'_a$	1.214	1.625	0.750	1.508	1.581
C(6′)	41.26	41.61	40.24	42.36	40.40
$H6'_e$	1.20	1.681	0.579	1.62	1.860
$H7'_{\psi a}$	1.168	1.499	1.162	1.462	1.85
C(7′)	53.16	53.3	52.76	53.3	55.29
$H7'_{\psi e}$	1.771	2.032	1.790	2.000	1.85
hba	Hα1: 1.403; 1.481		Hβ: 0.631; 0.786		Hγ: 3.025; 3.010
	Cα: 42.90		Cβ: 37.42		Cγ: 74.78

Table 2. *^{1}H-NMR Chemical-Shift Values of* **2** (relative to TMS) *in H_2O/C^2H_3CN 4 : 1 at 286 K*

	A_I	T_{II}	A_{III}	T_{IV}
NH		7.888	7.870	7.969
H2				
H8	8.090		8.121	
H6		7.372		7.502
H of Me		1.715		1.752
H1′	4.354	4.044	4.131	4.267
H2′	3.784	3.820	4.177	4.007
$H3'_a$	1.295	0.928	1.170	1.167
$H3'_e$	2.031	1.598	1.706	1.870
H4′	1.774	1.310	1.785	1.8?
$H5'_a$	0.974	0.272	1.013	1.108
$H5'_e$	1.176	0.120	1.332	1.758
$H6'_a$	1.911	1.215	1.948	1.641
$H6'_e$	1.888	1.394	2.005	1.808
$H7'_{\psi a}$	1.837	1.537	1.952	2.12
$H7'_{\psi e}$	2.161	1.952	2.075	2.12

indentified by a cross-peak to their respective thymidine Me groups (see *Fig. 8,a*), exhibit intraresidual cross-peaks to $H6'_e$ and $H6'_a$, as well as to H1′ and H2′. The remaining H8 signals of A_I and A_{III} in the 1D-NMR spectrum (*Fig. 6,a*), which can be recognized with certainty by their non-exchangeability with ^2H_2O, exhibit intraresidual cross-peak formation with H2′ and $H6'_a$ (*Fig. 9,b*). It is possible to correlate all of the cyclohexane ring protons up to and including the exocyclic protons $H7'_a$, $H7'_e$ with one another using TOCSY spectra with a mixing time of 80 ms. Since the signals of three H2′ protons are well-resolved in the 2D-COSY spectrum (*Fig. 8,a*), unambiguous assignment of the four NDAa residues is possible: the T_{II}-, A_{III}- and T_{IV}-containing NDAas may be determined directly, and the NDAa with A_I indirectly, by its missing amide proton. The exocyclic protons H7′(*pro-R*) and H7′(*pro-S*) may each be assigned thanks to a strong $H7'_{\psi a}$(*pro-R*) $(i-1)$/HN(i) cross peak in the ROESY spectrum, as well as the vicinal coupling constants of $^3J(H4',H7'_{\psi a}(pro\text{-}R) = 10.1$ Hz and ^3J(H4′, $H7'_{\psi e}(pro\text{-}S)) = 5.9$ Hz for T_{II}, of $^3J(H4',H7'_{\psi a}(pro\text{-}R)) = 8.8$ Hz and ^3J(H4′, $H7'_{\psi e}(pro\text{-}S)) = 6.5$ Hz for A_{III}, and of $^3J(H4',H7'_{\psi e}(pro\text{-}S)) = 6.0$ Hz for A_I.

Sequential assignment of the single strand is based on the three (boxed in *Fig. 9,b*) cross-peaks of the stereostructurally unambiguously assigned $H7'_{\psi a}(i-1)$ protons to the amide protons of A_{II}, T_{III}, and A_{IV}.

Fig. 9 shows a comparison of cross-peak intensities in the NOESY spectrum of duplex **(1)$_2$** and in the ROESY spectrum of single strand **2**. The weak cross-peak intensities in the NOESY spectrum of **2** at 286 and 295 K, from which may be inferred the presence of a monomer with a correlation time τ_c close to the NOE-zero crossover, is confirmed by the ROESY spectrum of **2** (*Fig. 9,b*).

In the NOESY spectrum of **(1)$_2$** (*Fig. 9,a*), unlike the ROESY spectrum of **2**, sequential cross-peaks of *both* exocyclic protons to the amide proton ($H7'_{\psi a}$/$H7'_{\psi e}(i-1)$/HN(i)) are observed. It is also noticeable that almost all the protons in the duplex are shifted to higher field compared with their counterpart resonances in the monomer.

2.3. *Conformational Analysis of* **(1)$_2$** *and* **2**. Of the six torsion angles in the δ-peptide repeating unit, only angles α, β, and ε are not fixed from the outset (see *Fig. 3*). Angles γ and δ are dictated by the cyclohexane ring, and ζ, which describes the conformation around the peptide bond, is fixed at a value of 180°.

The ^3J(H,H) values useful for conformational analysis for **(1)$_2$** and **2** may be found in *Table 3*.

Table 3. *Vicinal Homonuclear Coupling Constants of* **(1)$_2$** *and* **2**

(1)$_2$	A_I	A_{II}	T_{III}	A_{IV}	T_V
^3J(NH, H2′)	9.9	10.4	11.2	11.2	10.1
2	A_I	T_{II}	A_{III}	T_{IV}	
^3J(NH,H2′)		10.0	9.5	10.0	
$^3J(H4',H7'_a(pro\text{-}S))$		10.1	8.8		
$^3J(H4',H7'_e(pro\text{-}R))$	6.0	5.9	6.5		

Table 4 shows NOE cross-signals observed for **(1)$_2$**, classified into intraresidual or interresidual cross signals, the latter also broken down into intrastrand or interstrand cross signals.

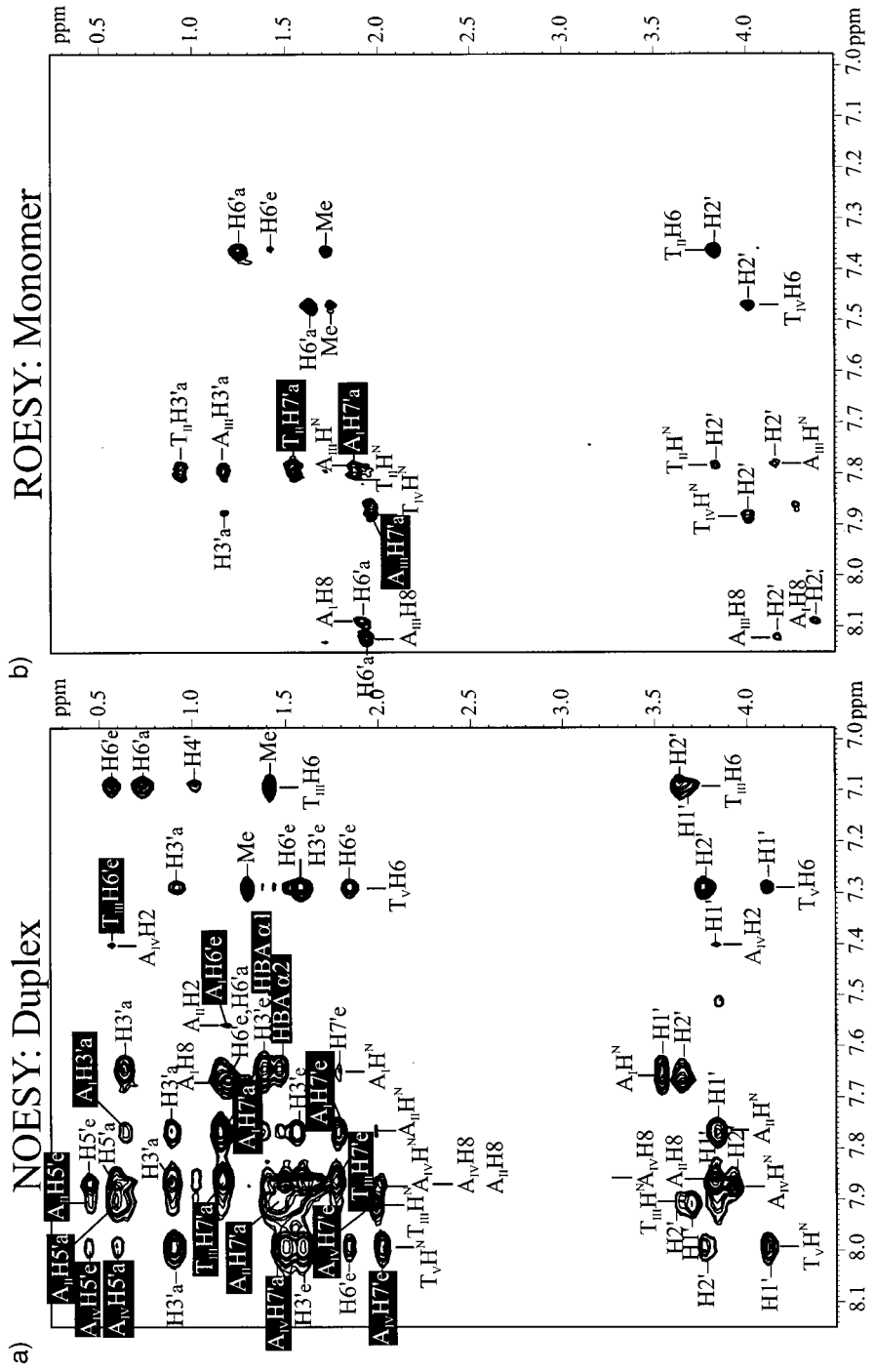

Fig. 9. *NOESY Spectrum of* $(\mathbf{1})_2$ (a) *and ROESY spectrum of* **2** (b) *in* ^2H_2O. The assigned cross peaks are indicated.

Table 4. *NOE Cross-peaks of* **(1)$_2$**, *Separated in* strong (*s*), medium (*m*) *and* weak (*w*) *Ones, Considering Proton-Proton Distances of* r = *2.2–2.8 Å* (*s*), *2.6–3.4 Å* (*m*), *or 3.2–6.0 Å* (*m*), *Respectively*

Resonance	Cross-peak to	Intensity	Resonance	Cross-peak to	Intensity
Intraresidual NOEs A_I					
A_I/NH	A_I/H1′	*s*	A_I/NH	A_I/H2′	*m*
A_I/NH	A_I/H3′$_e$	*m*	A_I/NH	A_I/H3′$_a$	*s*
A_I/NH	A_I/H5′$_e$	*w*	A_I/NH	A_I/H5′$_a$	*w*
A_I/NH	A_I/H6′$_e$	*w*	A_I/NH	A_I/H8	*w*
A_I/H8	A_I/H1′	*w*	A_I/H8	A_I/H2′	*s*
A_I/H8	A_I/H5′$_e$	*w*	A_I/H8	A_I/H5′$_a$	*w*
A_I/H8	A_I/H6′$_e$	*m*	A_I/H8	A_I/H6′$_a$	*s*
Interresidual, intrastrand NOEs A_I					
A_I/NH	HBA/H$_a$	*m*	A_I/NH	HBA/H$_b$	*m*
A_I/H8	A_{II}/NH$_2$	*w*			
Interresidual, interstrand NOEs A_I n.d.					
Interresidual NOEs A_{II}					
A_{II}/NH	A_{II}/H1′	*s*	A_{II}/NH	A_{II}/H2′	*m*
A_{II}/NH	A_{II}/H3′$_e$	*m*	A_{II}/NH	A_{II}/H3′$_a$	*s*
A_{II}/NH	A_{II}/H5′$_e$	*w*	A_{II}/NH	A_{II}/H5′$_a$	*w*
A_{II}/NH	A_{II}/H6′$_e$	*w*	A_{II}/NH	A_{II}/H8	*w*
A_{II}/H8	A_{II}/H1′	*w*	A_{II}/H8	A_{II}/H2′	*s*
A_{II}/H8	A_{II}/H5′$_e$	*w*	A_{II}/H8	A_{II}/H5′$_a$	*w*
A_{II}/H8	A_{II}/H6′$_e$	*m*	A_{II}/H8	A_{II}/H6′$_a$	*s*
Interresidual, interstrand NOEs A_{II}					
A_{II}/NH	A_I/H5′$_e$	*m*	A_{II}/NH	A_I/H5′$_a$	*m*
A_{II}/NH	A_I/H7′$_e$	*m*	A_{II}/NH	A_I/H7′$_a$	*s*
A_{II}/H8	A_I/H5′$_e$	*w*	A_{II}/H8	A_I/H5′$_a$	*w*
A_{II}/H2	A_I/H1′	*w*	A_{II}/H2	A_I/H5′$_e$	*w*
A_{II}/H2	A_I/H5′$_a$	*w*	A_{II}/H2	A_I/H6′$_e$	*w*
A_{II}/H2	A_I/H6′$_a$	*w*			
Interresidual, interstrand NOEs A_{II}					
A_{II}/NH$_2$	T_V/H3	*w*	A_{II}/NH$_2$	T_V/H7	*w*
A_{II}/NH$_2$	A_{IV}/H6′$_e$	*w*	A_{II}/NH$_2$	A_{IV}/H6′$_a$	*w*
A_{II}/NH$_2$	A_{IV}/H5′$_e$	*w*	A_{II}/NH$_2$	A_{IV}/H5′$_a$	*w*
A_{II}/H$_2$	A_{IV}/H1′	*w*	A_{II}/H8	A_{IV}/NH$_2$	*w*
Intraresidual NOEs T_{III}					
T_{III}/NH	T_{III}/H1′	*s*	T_{III}/NH	T_{III}/H2′	*m*
T_{III}/NH	T_{III}/H3′$_e$	*m*	T_{III}/NH	T_{III}/H3′$_a$	*s*
T_{III}/NH	T_{III}/H5′$_e$	*w*	T_{III}/NH	T_{III}/H5′$_a$	*w*
T_{III}/NH	T_{III}/H6′$_e$	*w*	T_{III}/NH	T_{III}/H6	*w*
T_{III}/H6	T_{III}/H1′	*w*	T_{III}/H8	T_{III}/H2′	*s*
T_{III}/H6	T_{III}/H5′$_e$	*w*	T_{III}/H8	T_{III}/H5′$_a$	*w*
T_{III}/H6	T_{III}/H6′$_e$	*m*	T_{III}/H8	T_{III}/H6′$_a$	*s*
Interresidual, intrastrand NOEs T_{III}					
T_{III}/NH	A_{II}/H5′$_e$	*m*	T_{III}/NH	A_{II}/H5′$_a$	*m*
T_{III}/NH	A_{II}/H7′$_a$	*s*	T_{III}/H6	A_{II}/H5′$_e$	*w*
T_{III}/H3	A_{II}/H6′$_e$	*m*	T_{III}/H3	A_{II}/H6′$_a$	*w*
Interresidual, interstrand NOEs T_{III}					
T_{III}/H3	T_{III}/H6′$_e$	*w*	T_{III}/H3	T_{III}/H6′$_a$	*w*
Intraresidual NOEs A_{IV}					
A_{IV}/NH	A_{IV}/H1′	*s*	A_{IV}/NH	A_{IV}/H2′	*m*
A_{IV}/NH	A_{IV}/H3′$_e$	*m*	A_{IV}/NH	A_{IV}/H3′$_a$	*s*
A_{IV}/NH	A_{IV}/H5′$_e$	*w*	A_{IV}/NH	A_{IV}/H5′$_a$	*w*
A_{IV}/NH	A_{IV}/H6′$_e$	*w*	A_{IV}/NH	A_{IV}/H8	*w*

Table 4 (cont.)

Resonance	Cross-peak to	Intensity	Resonance	Cross-peak to	Intensity
A_{IV}/H8	A_{IV}/H1′	*w*	A_{IV}/H8	A_{IV}/H2′	*s*
A_{IV}/H8	A_{IV}/H5′$_e$	*w*	A_{IV}/H8	A_{IV}/H5′$_a$	*w*
A_{IV}/H8	A_{IV}/H6′$_e$	*m*	A_{IV}/H8	A_{IV}/H6′$_a$	*s*
A_{IV}/H8	A_{IV}/H4′	*w*			
Interresidual, intrastrand NOEs A_{IV}					
A_{IV}/NH	T_{III}/H5′$_e$	*m*	A_{IV}/NH	T_{III}/H5′$_a$	*m*
A_{IV}/NH	T_{III}/H7′$_e$	*m*	A_{IV}/NH	T_{III}/H7′$_a$	*s*
A_{IV}/H8	T_{III}/H5′$_e$	*w*	A_{IV}/H8	T_{III}/H5′$_a$	*w*
A_{IV}/H2	T_{III}/H1′	*w*	A_{IV}/H2	T_{III}/H5′$_e$	*w*
A_{IV}/H2	T_{III}/H5′$_a$	*w*	A_{IV}/H2	T_{III}/H6′$_e$	*w*
A_{IV}/H2	T_{III}/H6′$_a$	*w*	A_{IV}/NH_2	T_{III}/H7′	*w*
A_{IV}/NH_2	T_{III}/H6	*w*			
Interresidual, interstrand NOEs A_{IV}					
A_{IV}/NH_2	T_{III}/H3	*w*	A_{IV}/NH_2	T_{III}/H7	*w*
A_{IV}/NH_2	A_{III}/H6′$_e$	*w*	A_{IV}/NH_2	A_{II}/H6′$_a$	*w*
A_{IV}/NH_2	A_{III}/H5′$_e$	*w*	A_{IV}/H2	A_{IV}/H1′	*w*
A_{IV}/NH_2	A_{II}/H8′$_e$	*w*			
A_{IV}/H8	A_{II}/NH_2	*w*			
Intraresidual NOEs T_V					
T_V/NH	T_V/H1′	*s*	T_V/NH	T_V/H2′	*m*
T_V/NH	T_V/H3′$_e$	*m*	T_V/NH	T_V/H3′$_a$	*s*
T_V/NH	T_V/H5′$_e$	*w*	T_V/NH	T_V/H5′$_a$	*w*
T_V/NH	T_V/H6′$_e$	*w*	T_V/NH	T_V/H8	*w*
T_V/H6	T_V/H1′	*w*	T_V/H6	T_V/H2′	*s*
T_V/H6	T_V/H5′$_e$	*w*	T_V/H6	T_V/H5′$_a$	*w*
T_V/H6	T_V/H6′$_e$	*m*	T_V/H6	T_V/H6′$_a$	*s*
Interresidual, intrastrand NOEs T_V					
T_V/NH	A_{IV}/H5′$_e$	*m*	T_V/NH	A_{IV}/H5′$_a$	*m*
T_V/NH	A_{IV}/H7′$_e$	*m*	T_V/H6	A_{IV}/H7′$_a$	*s*
T_V/H6	A_{IV}/H5′$_e$	*w*	T_V/H6	A_{IV}/H5′$_a$	*w*

Torsion angle ε may be obtained with the aid of the 1D-^{1}H-NMR spectrum coupling between HN and the H2′ proton (*Fig. 6*). Since ^3J(HN,H2′) is *ca.* 10 Hz (see *Table 3*), the two intercoupling protons must lie *ap* to one another; *i.e.*, $\varepsilon \approx 120°$. The relatively strong NOE cross-peaks from the amide proton HN to the axial H3′$_a$, compared with the similarly observed but weaker (HN/H3′$_e$)-NOE cross-peak is in agreement with this.

Efforts to determine the torsion angle β in duplex **(1)$_2$** make use of the ^3J(H,H) values (*Table 3*) determined for the tetramer **2**, with the aid of which the torsion angle between the bonds from H4′ to C(4) and from H7′$_{\psi a}$ to C(7) can be calculated. In the case of **(1)$_2$**, overlapping of resonance signals prevents direct ascertainment of the vicinal coupling constants. In the COSY spectrum (*Fig. 8*), one of the diastereotopic H7′ protons shows a large coupling constant of 9–10 Hz (*ap*-orientation), the other a small one of 6 Hz (*sc*-orientation). This points to a suspected fixed value for β (see *Sect. 1.3*). According to this, torsion angle β is *ca.* 180°. In anticipation of the (still to be discussed) calculation of the structure of **(1)$_2$** (*vide infra*), it should be mentioned here that a duplex structure can only arise if angle β adopts a value of *ca.* 180°. Put another

way, the exocyclic CH_2 group appears to be a relatively rigid extension of the cyclohexane ring. It is only logical that this does not apply for the flexible C-terminal carboxymethyl group of T_{IV} in **2**, whose protons are isochronous. It is also not surprising that, in each case, only one pronounced NOE cross-signal between HN and the $H7'_{\psi a}$ proton of the preceding repeating unit is observed. For torsion angle α, this therefore yields a value of *ca.* $-120°$.

Just as the resonance signals of the equatorial protons of the cyclohexane are, as a rule, shifted to lower field relative to those of the axial protons (with the exception of the $H5'_a/H5'_e$ protons discussed above), the resonance signals of the $H7'_{\psi e}$ protons are found at lower field than those of the $H7'_{\psi a}$ protons. The difference in chemical shift is, at 0.58 ppm, more pronounced in the duplex than in the tetramer single strand (0.29 ppm). This leads to the conclusion that the conformational averaging between the three staggered conformations (*Scheme*) is less pronounced in $\mathbf{(1)_2}$ than in **2**.

Scheme

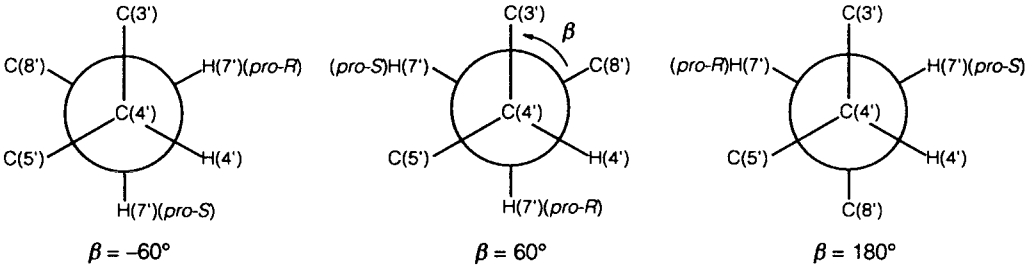

The *anti*-conformation about the exocyclic angle χ, is settled unambiguously by the observed strong intraresidual NOE cross signals H8/H2′ and $H8/H6'_a$ for A, and H6/H2′ and $H6/H6'_a$ for T.

3. NMR Structure Calculation of Duplex $\mathbf{(1)_2}$ Using MD Search of Torsion-Angle Space. – A NMR structure-calculation method has been applied here, which uses MD constrained to torsion-angle space [13]. A major advantage of this torsion-angle MD method is its simplicity. The followed protocol consists of few stages, four in this case, with only two parameters changing: ω_{vdw} and $\omega_{\text{dihedral.}}$

3.1. *Methods.* The structure of duplex $\mathbf{(1)_2}$ was calculated (see *Exper. Part*) starting from two randomized single-strand conformations using a modified simulated annealing protocol with the X-PLOR 98.1 program [22] in torsion-angle space [13][23]. Different random starting conformations (for ensembles **A**, **B**, and **C**; *vide infra*) were generated using a torsion-angle randomization BCL script in the INSIGHT II program [24] followed by 100 steps of conjugate gradient minimization.

The structure calculation is outlined in *Table 5*. The published protocol [13] was modified by omitting the slow-cooling Cartesian MD step and adding an extra step of minimization at the end of the refinement using full *Lennard-Jones* non-bonding potentials and dihedral terms. Also, for minimization we used the recently implemented Adopted-Basis *Newton-Raphson* (ABNR) method [22] instead of the *Powell*

Table 5. *Torsion-Angle Molecular-Dynamics Protocol*. The weights for *van der Waals* interaction (ω_{vdw}), NOE-derived distance restraints (ω_{NOE}), and dihedral-angle restraints derived from *J* coupling-constant measurement ($\omega_{dihedral}$) are used in energy functions described in [13].

	Stage 1	Stage 2	Stage 3	Stage 4
High-temperature torsion-angle MD	Slow-cooling torsion-angle MD	2000 steps ABNR minimization	2000 steps ABNR minimization	
Temp	20000 K	20000 K → 0 K	–	–
Time step	0.015 ps	0.015 ps	–	–
Time	60 ps	60 ps	–	–
ω_{NOE}	150	150	5	5
$\omega_{dihedral}$	5	5	100	100
ω_{vdw}	0.1	0.1 → 1.0	1.0	1.0
Non-bonding interactions	repel	repel	repel	*Lennard-Jones*

method. It was shown that the ABNR method can more efficiently avoid being trapped in local minima by using second derivatives.

A force constant of 370 kcal · mol^{-1} · Å^{-2} was used for the amide bond identical to that one employed in protein structure calculation. Distance (1.9 ± 0.3 Å) and force constant (150 kcal · mol^{-1} · Å^{-2}) for the geometry of the H-bond in the base pair were chosen identical to the values for base pairing in oligonucleotide structure calculation. The same is true for the force constant to keep the bases planar (400 kcal · mol^{-1} · Å^{-2}). The CHARMM 22 potential [25] was used.

3.2. *Results and Discussion*. The results of the structure calculation of **(1)$_2$** are presented in *Table 6*.

Statistics were generated by choosing the 10 best structures (according to NOE and torsion-angle violations) among the first 20 generated ones. *Fig. 10* shows superpositions of ensembles in each case of the 10 best converged structures.

Table 6. *Experimental Restraints and Statistics of Structures*

Experimental Restraints	
NOE-derived distance restraints	136
intraresidual	72
intrastrand	39
interstrand	17
Hydrogen bond, base-planarity, and peptide-bond *constraints*	13
Torsion-angle *restraints*	5
Total experimental *restraints*	146
Mean number per NDAa residue	29.2
Statistics of Final Structure	
Number of minimized structures	20
Mean NOE deviation of convergent structures (> 0.2 Å)	0
Torsion-angle deviation in convergent structures (> 5°)	0
R.m.s. deviations from mean structure [Å]	
Ensemble **AI** (start structure I, no *β-restraint*)	1.6
Ensemble **AII** (start structure I, ± 10° *β-restraint*)	0.96
Ensemble **AIII** (start structure I, ± 30° *β-restraint*)	0.83
Ensemble **B** (start structure II, ± 30° *β-restraint*)	0.82
Ensemble **C** (start structure III, ± 30° *β-restraint*)	0.80

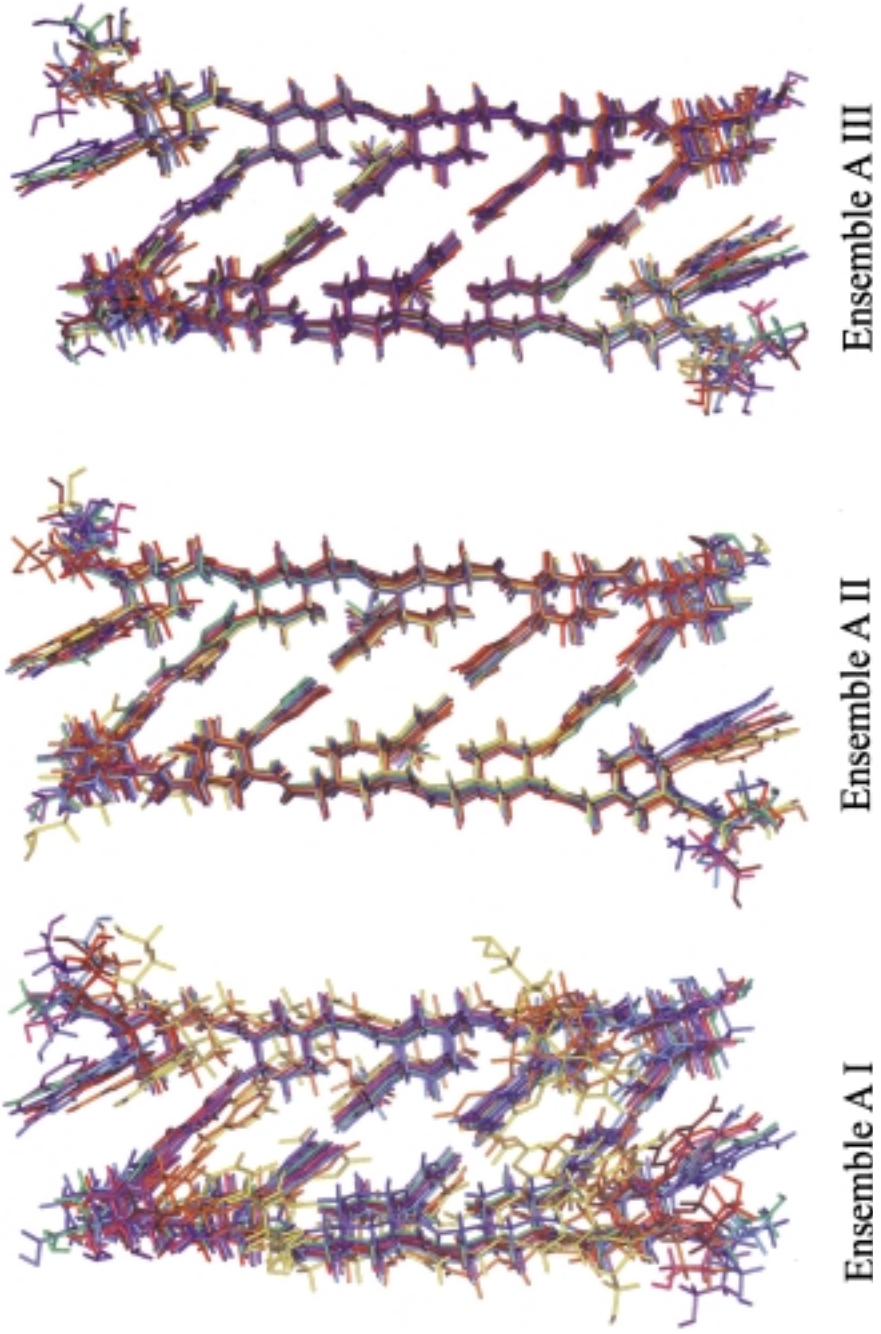

Fig. 10. *Superposition of simulated annealing structures in ensembles* **AI**, **AII**, *and* **AIII**

Ensembles **AI**, **AII**, and **AIII** have the same starting conformation, but differ in torsion-angle restraints. In ensemble **AI**, torsion angle β was left unrestrained. As analysis of homonuclear coupling constants (see *Sect. 2.2*) suggested a figure for β of *ca.* 180°, this torsion angle was restrained to $180 \pm 10°$ (**AII**) or $180 \pm 30°$ (**AIII**), respectively. In additional calculations (for different random starting conformations used in ensembles **B** and **C**, the data of which are not shown), identical parameters as in the calculation for ensemble **AIII** were employed. The convergence clearly depends on the incorporation of a β-restraint. The root mean square (r.m.s) deviations, summarized in *Table 6* for the structure with the β-restrained violation of $\pm 10°$ is slightly higher than for structures with β-restrained violation of $\pm 30°$, suggesting an overrestraint in the former ensemble. The same trend is observed for the torsion angle α, summarized in *Table 7:* in ensemble **AI** the variation of torsion angles α and β is considerably higher than in the other ensembles.

Table 7. *Torsion Angles for Various Ensembles of Calculated Structures*

	Ensemble **AI**	Ensemble **AII**	Ensemble **AIII**	Ensemble **B**	Ensemble **C**
α	$122.9 \pm 20°$	$128.2 \pm 1.5°$	$128.7 \pm 1.3°$	$128.5 \pm 1.6°$	$128.7 \pm 1.3°$
β	$141.9 \pm 80°$	$169.2 \pm 2.3°$	$167.8 \pm 2.5°$	$167.5 \pm 2.9°$	$167.5 \pm 2.7°$
γ	$169.5 \pm 4.2°$	$170.8 \pm 2.7°$	$169.9 \pm 3.1°$	$170.0 \pm 3.1°$	$169.9 \pm 2.8°$
δ	$175.0 \pm 4.5°$	$176.5 \pm 3.2°$	$175.8 \pm 3.3°$	$176.2 \pm 3.4°$	$176.3 \pm 3.1°$
ε	$111.1 \pm 9°$	$125.5 \pm 7°$	$124.7 \pm 6.5°$	$123.4 \pm 7.5°$	$123.8 \pm 8.5°$
ζ	$179.0 \pm 7.8°$	$179.1 \pm 7.5°$	$179.1 \pm 7.6°$	$179.0 \pm 8.1°$	$179.1 \pm 7.4°$

The self-pairing single strands (1′*S*,2′*S*,4′*S*)-(phba)-NDP($A_IA_{II}T_{III}A_{IV}T_V$) form the duplex **(1)$_2$**. *Fig. 11* shows the structure that has the lowest energy.

Duplex **(1)$_2$** is stabilized by *1*) *Watson-Crick* H-bonds between the four pairs of complementary nucleobase residues: A_{II}-T_V, T_{III}-A_{IV}, A_{IV}-T_{III}, T_V-A_{II}; *2*) interstrand purine-purine stacking between A_{II} or A_{IV} of one, and A_{IV} or A_{II} of the other strand; *3*) interstrand purine-pyrimidine stacking between A_I or T_V of one, and T_V or A_I of the other strand.

Both, duplex [(1′*S*,2′*S*,4′*S*)-(phba)-NDP(AATAT)]$_2$ (**(1)$_2$**) and duplex [β-D-ribopyranosyl-(2′–4′)-(CGAATTCG)]$_2$ [11c] have the same inclination of *ca.* –50°[14]) and, not surprisingly at all, do hybridize (see *Part 3* [2]). Such a strong inclination puts neighboring bases, belonging to opposite strands, into a relative position well-suited for the just mentioned interstrand stackings between two nucleobases. A-A interstrand interaction is substantial because of the rigid arrangement of these nucleobases and a difference of *ca.* 5.9 Å only between strongly overlapping A residues (*Fig. 12*).

T-T Interstrand interaction leads to a reduced overlap compared with A-A interstrand interaction, and the net stacking effect, as determined from melting-curve analysis [2] is small, if present at all. The dangling-end residue A_I, lacking a complementary partner for pairing, even in solution is not completely flexible (*Fig. 13*) because of interstrand stacking to T_V, hereby stabilizing the duplex, provided the unpaired NDAa occupies the N terminus.

[14]) For specification of inclination (direction and degree), see [26].

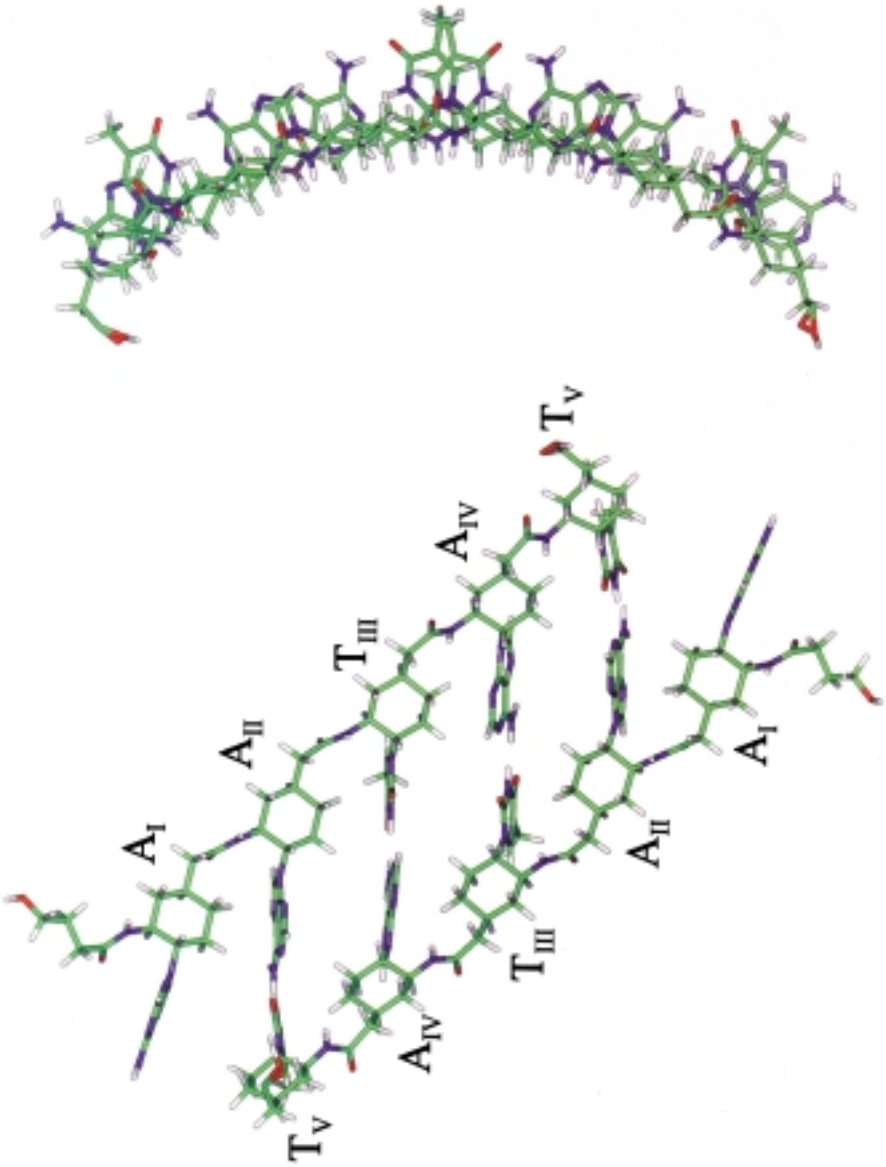

Fig. 11. *The least-energy structure of duplex* **(1)**$_2$ *for torsion-angle MD*

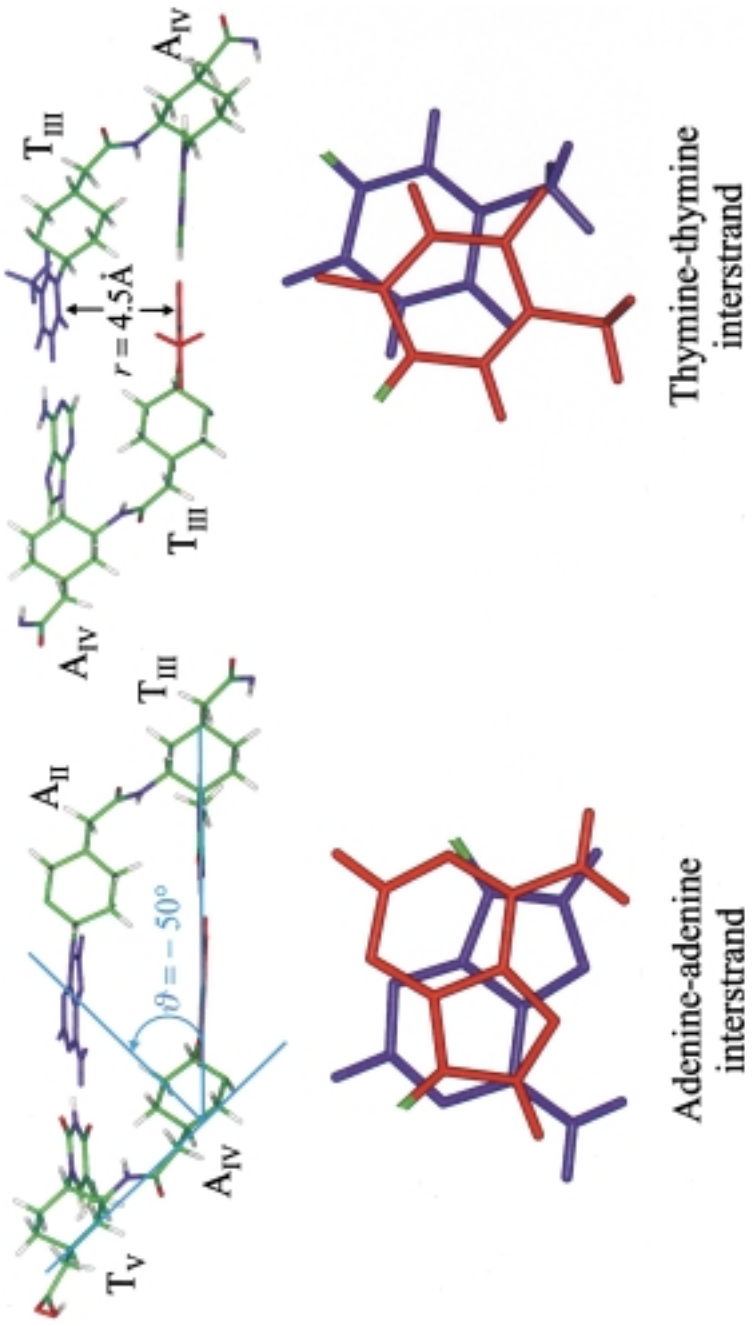

Fig. 12. *Adenin-adenin and thymin-thymin interstrand stackings* (side and top view) *with information about inclination* [26] *and distance between bases on opposite strands*

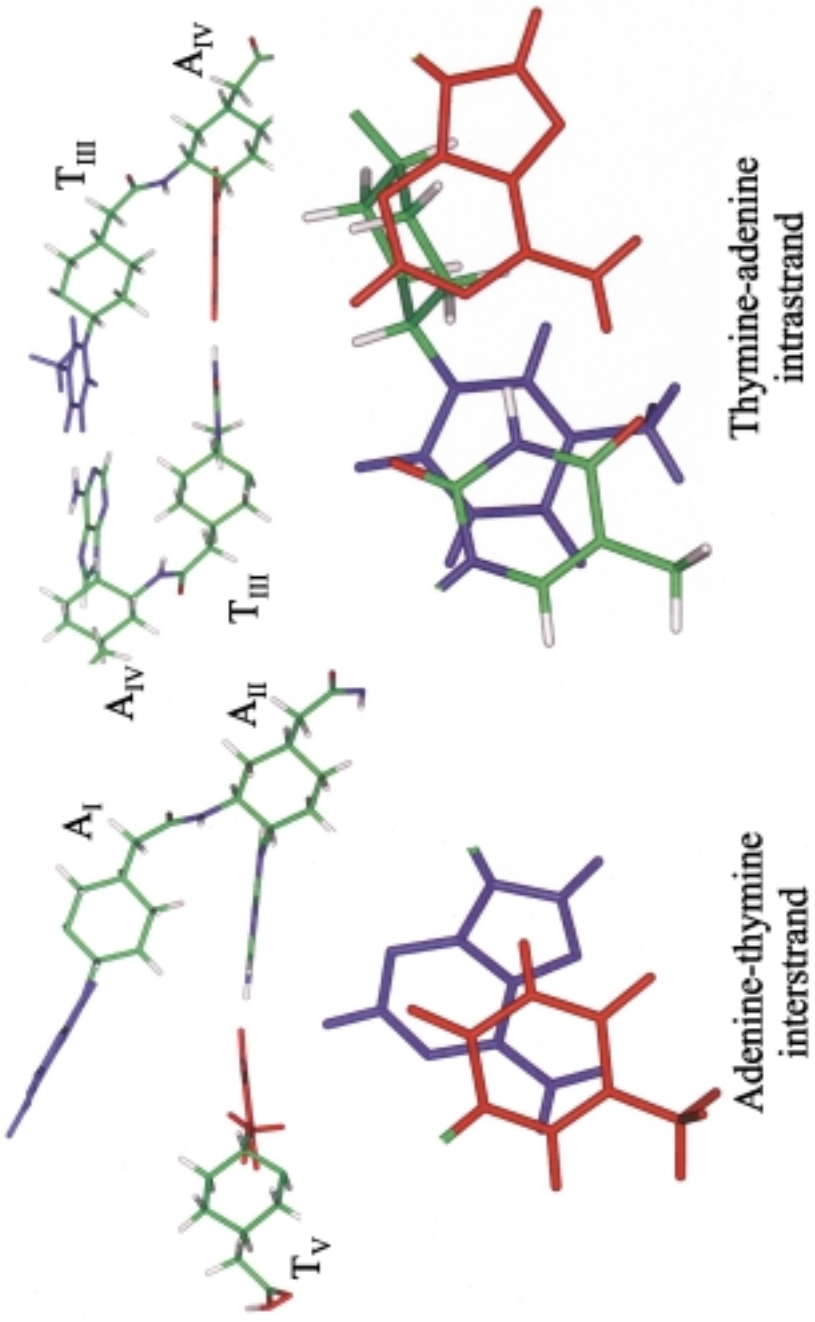

Fig. 13. *Adenin-thymin interstrand and thymin-adenin intrastrand stackings* (side and top view)

Slight deviation, in the case of **(1)$_2$**, from the linear-idealized conformation (see torsion angles in *Fig. 3*) leads to a right-handed double-helix with *Watson-Crick* base pairs. This double-helix has a unit twist of *ca.* $10 \pm 2^\circ$ and a unit height of 7.5 ± 0.1 Å. The corresponding figures for p-RNA are *ca.* 20° (unit twist) and *ca.* 6.0 ± 0.5 Å (unit height) [11c]. The smaller helicity of NDP relative to p-RNA, at least in part, is due to the lower flexibility of the backbone in the former case. This has to do with the number of freely rotating bonds in the acyclic portions of these molecules: p-RNAs have four bonds of this type between each two adjacent rings, NDPs have only three. The term 'freely rotating bonds' can easily make a false impression. As NMR analysis at or below room temperature reveals, the preferred NDP-oligomer conformation comes close to the three-dimensional arrangement shown in *Fig. 4*.

The change of single-strand topography on duplex formation is smaller for NDP than for p-RNA, or to put in another way, NDPs are better preorganized for this kind of association than p-RNAs. This view is convincingly supported by a series of NMR data already presented. This may contribute to the greater stability of NDP compared to p-RNA duplexes. The absence of repulsive electrostatic interactions in the former, which are typical for the latter, however, should not be overlooked.

4. Conclusion. – The conclusion drawn from the NMR and MD studies of a p-RNA duplex [11c] is very similar to the inference from the present investigation of a NDP duplex. The self consistancy of the structural details derived from NMR data (*Chapt. 2*), together with the least-energy structure calculated (*Chapt. 3*), indicate that a single conformation type of the NDP duplex dominates in solution, and that no other backbone conformations are low enough in energy to have important statistical-mechanical weight. Both, the NMR-derived conformational model (*Figs. 4* and *7*) and the least-energy MD structure (*Fig. 11*) confirm the main structural features predicted by qualitative conformational analysis (*Sect. 1.3*). A duplex is formed by antiparallel arrangement of two complementary strands and stabilized by *Watson-Crick* base pairing due to the H-bonding and interstrand π-π base stacking, dangling-end nucleobase interaction included. On the basis of the reported structural details, functional devices growing out of them are behold right ahead [27].

This work was supported by the German *Bundesministerium für Bildung, Wissenschaft, Forschung und Technologie* (Project No. 0311030). We thank Drs. *W. Bermel* and *R. Kerssebaum, Bruker*, Karlsruhe, for NMR measurement time. We are pleased to acknowledge Prof. *Christian Griesinger* for stimulating discussions. *H.S.* was supported by the *European Union* (ERBFMGECT 950034). Dr. *Andrew Beard* kindly took care of the English.

Experimental Part

The *preparation of oligomers* **1** and **2** will be described in *Part 3* [2]. *NMR Experiments* were performed on *Bruker DRX 500*, *DRX 600*, and *DRX 800* spectrometers equipped with *TXE* ^{1}H, ^{13}C, ^{15}N probes with actively shielded gradients at *Bruker Analytik GmbH*, Karlsruhe, and at the *European Large-Scale NMR Facility*, Frankfurt a.M. The sample concentration was 1 mM in H_2O for **(1)$_2$** and 0.5 mM in H_2O/C^2H_3CN for **2**. In the latter case, the ^{2}H signal of the solvent was used as lock signal. The imino resonances were observed in a jump-return echo sequence [20a]. The NOESY spectra of **(1)$_2$** in $H_2O/^2H_2O$ 9:1 were optimized to suppress the radiation damping of water. First, a water flip-back pulse [28] (rectangle pulse with $\gamma B/2\pi = 50$ Hz) was used before the excitation pulse and after the 90° pulse that starts the NOESY mixing time. The first water flip-back pulse was cycled 180° out of phase with the excitation pulse according to the STATES-TPPI scheme [29]. Secondly, radiation damping was suppressed by applying weak bipolar gradients [30] in t_1 and a weak gradient during the mixing time. The strength of the gradients is given in *Fig. 14.*

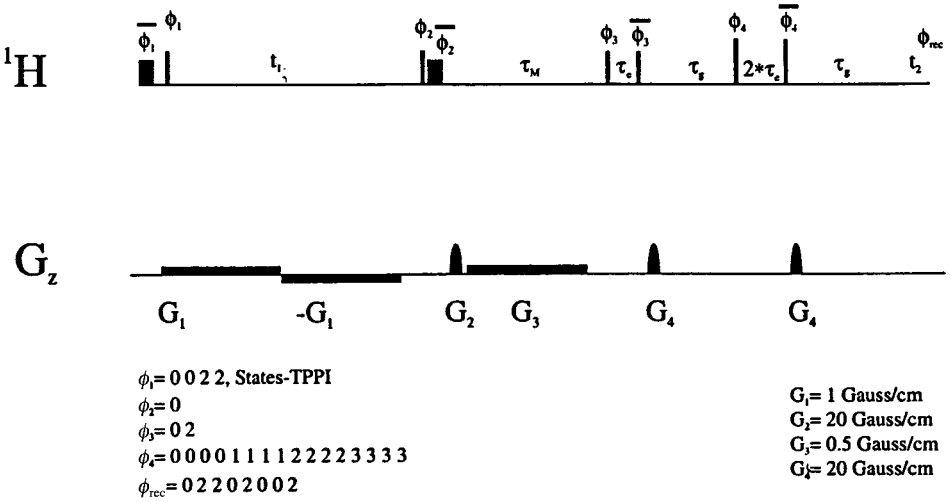

Fig. 14. *Pulse sequence for the NOESY experiment to suppress radiation damping*

Recording and processing parameters for **(1)$_2$** and **2** are given in *Table 8*.

Restrained MD Structure Calculation. Contrary to **(1)$_2$**, in the case of **2** the number of experimental NMR constraints (distance and dihedral angles) was not sufficient to allow NMR-structure calculation. All the calculations (see *Sect. 3.1*) were done on a *SGI Origin 200* computer. The preparation stage consisted of 4000

Table 8. *Details of Performance of NMR Experiments*

(1)$_2$	B_0 [MHz]	T [K]	TD1[a]) / TD2	SW1[b]) / SW2 [Hz]	d[c]) [s]	NS[d])	SI1[e]) / SI2
NOESY	506.132	277	600	10000	2.5	64	1024
			4096	10000			4096
TOCSY	600.132	277	800	8012.8	2.0	32	1024
			4096	8012.8			4096
COSY	600.132	277	800	8012.8	2.0	32	1024
			4096	8012.8			4096
HSQC	599.873	277	384	10000.0	1.4	256	1024
	150.846		2048	15084.5			4096
2	B_0 [MHz]	T [K]	TD1[a]) / TD2	SW1[b]) / SW2 [Hz]	d[c]) [s]	NS[d])	SI1[e]) / SI2
ROESY	600.141	300	600	8196.7	1.5	64	1024
			4096	8196.7			4096
TOCSY	600.141	300	592	7575.8	1.5	32	1024
			4096	8196.7			4096
COSY	500.133	286	1024	6361.3	2.0	128	1024
			4096	6361.3			4096

[a]) Number of real time-domain data points in 2 dimensions. [b]) Spectral width for two dimensions. [c]) Delay time between transients. [d]) Number of transients along the time axis the FID is observed. [e]) Number of real data points for two dimensions.

steps high-temperature torsion-angle dynamics sampling at 20000 K, applying a reduced non-bonding interaction with hard-sphere repulsion with a scaled down force constant for heavy atoms, and no force acting in pairs involving H-atoms. This was followed by a slow cooling stage from 20000 K to 0 K in 4000 steps, during which the non-bonding interaction was sealed back. The NOE force constant during these two stages was kept constant at 150 kcal · mol^{-1} · Å^{-2}. After the MD stages, the structures were minimized first using the repel non-bonding potential for 2000 steps, and then the *Lennard-Jones* non-bonding potential was turned on, and a second stage of minimization was carried out for 2000 steps.

NOE Restraints were averaged using the $\langle r^{-6} \rangle$ averaging as implemented in X-PLOR. A total of 136 NOE-derived distance restraints, 5 planarity constraints for the basepairs and 5 torsion-angle restraints derived from ^3J(H,H) values were incorporated (see *Table 6*).

REFERENCES

[1] G. Karig, A. Fuchs, A. Büsing, T. Brandstetter, S. Scherer, J. W. Bats, A. Eschenmoser, G. Quinkert, *Helv. Chim. Acta* **2000**, *83*, 1049.
[2] S. Kienle, S. Feiertag, J. Wermuth, N. Windhab, M. Pignot, J. Müller, A. Eschenmoser, G. Quinkert, *Helv. Chim. Acta* **2000**, *83*, in preparation.
[3] Jochen Wermuth, BMBF Projekt 0311030; Postdoctoral research report 1998.
[4] Christian Richter, Ph.D. Thesis, University of Frankfurt, 2000.
[5] H. Kessler, M. Gehrke, C. Griesinger, *Angew. Chem., Int. Ed.* **1988**, *27*, 490.
[6] M. Bolli, R. Micura, S. Pitsch, A. Eschenmoser, *Helv. Chim. Acta* **1997**, *80*, 1901.
[7] K. Groebke, J. Hunziker, W. Fraser, L. Peng, U. Diederichsen, K. Zimmermann, A. Holzner, C. Leumann, A. Eschenmoser, *Helv. Chim. Acta* **1998**, *81*, 375; 399.
[8] G. Quinkert, E. Egert, C. Griesinger, 'Aspects of Organic Chemistry' Verlag Helvetica Chimica Acta, Basel, 1996.
[9] F. Johnson, *Chem. Rev.* **1968**, *68*, 375.
[10] R. W. Hoffmann, *Chem. Rev.* **1989**, *89*, 1841.
[11] a) S. Pitsch, S. Wendeborn, B. Jaun, A. Eschenmoser, *Helv. Chim. Acta* **1993**, *76*, 2161; b) S. Pitsch, R. Krishnamurthy, M. Bolli, S. Wendeborn, A. Holzner, M. Minton, C. Lesueur, I. Schlönvogt, B. Jaun, A. Eschenmoser, *Helv. Chim. Acta* **1995**, *78*, 1621; c) I. Schlönvogt, S. Pitsch, C. Lesueur, A. Eschenmoser, B. Jaun, R. M. Wolf. *Helv. Chim. Acta* **1996**, *79*, 2316; d) A. Eschenmoser, *Science* **1999**, *284*, 2118.
[12] R. Micura, R. Kudick, S. Pitsch, A. Eschenmoser, *Angew. Chem.*, *Int. Ed*. **1999**, *38*, 680.
[13] a) E. G. Stein, L. M. Rice, A. T. Brünger, *J. Magn. Reson.* **1997**, *124*, 154; b) A. T. Brünger, X-PLOR: A system for X-ray crystallography and NMR; Yale University, New Haven, Conn., 1996.
[14] K. Wüthrich, NMR of Proteins and Nucleic Acids, John Wiley & Sons, New York, 1986.
[15] M. A. Viswamitra, Z. Shakked, P. G. Jones, G. M. Sheldrick, S. A. Salisbury, O. Kennard, *Biopolymers* **1982**, *21*, 513.
[16] W. P. Aue, E. Bartholdi, R. R. Ernst, *J. Chem. Phys.* **1976**, *64*, 2229.
[17] L. Braunschweiler, R. R. Ernst, *J. Magn. Reson*. **1983**, *53*, 521.
[18] A. A. Bothner-By, R. L. Stephens, J.-M. Lee, C. D. Warren, R. W. Jeanloz, *J. Am. Chem. Soc*. **1984**, *106*, 811.
[19] a) J. Jeener, B. H. Meier, P. Bachmann, R. R. Ernst, *J. Chem. Phys.* **1979**, *71*, 4546; b) S. Macura, Y. Huang, D. Suter, R. R. Ernst, *J. Magn. Reson.* **1981**, *43*, 259.
[20] a) V. Sklenar, A. Bax, *J. Magn. Reson*. **1987**, *74*, 469; b) G. Bodenhausen, D. J. Ruben, *Chem. Phys. Lett*. **1980**, *69*, 185.
[21] R. U. Lemieux, R. K. Kullnig, H. J. Bernstein, W. G. Schneider, *J. Am. Chem. Soc*. **1958**, *80*, 6098.
[22] J. Badger, R. A. Kumar, P. Yip, S. Szalma, *Proteins* **1999**, *35*, 25.
[23] L. M. Rice, A. T. Brünger, *Proteins* **1994**, *19*, 277.
[24] Insight II, MSI, San Siego, 1998.
[25] A. D. MacKerell, Jr., J. Wiorkiewicz-Kuczera, M. Karplus, *J. Am. Chem. Soc*. **1995**, *117*, 11946.
[26] M. Egli, P. Lubini, M. Bolli, S. Pitsch, A. Eschenmoser, in preparation.
[27] G. Quinkert, *Verh. Ges. Dtsch. Naturforsch. Ärzte* **1999**, *120*, 163.
[28] S. Grzesiek, A. Bax, *J. Am. Chem. Soc*. **1993**, *115*, 12593.
[29] D. Marion, M. Ikura, R. Tschudin, A. Bax, *J. Magn. Reson.* **1989**, *85*, 393.
[30] V. Sklenar, *J. Magn. Reson., Ser. A* **1995**, *114*, 132.

Received November 23, 1999